1998

Mineralogy and geochemistry of Bay of Bengal deep-sea fan sediments, ODP Leg 116: evidence for an Indian subcontinent contribution to distal fan sedimentation

STEPHEN F. CROWLEY[1], DORRIK A. V. STOW[2] & IAN W. CROUDACE[2]

[1] *Department of Earth Sciences, University of Liverpool, PO Box 147, Liverpool L69 3BX, UK*

[2] *Department of Geology, University of Southampton, Southampton SO9 5ND, UK*

Abstract: Sediments recovered during Ocean Drilling Program Leg 116 (Bay of Bengal deep-sea fan) fall into three mineralogically and geochemically distinct groups. The first of these groups (Group I), characterized by quartz–mica-rich turbidites, constitutes the largest proportion of distal fan sediments. Trace element patterns are similar to modern River Ganges suspended sediment and are consistent with a Himalayan (meta)sedimentary/granitic source. The second group of sediments (Group II) is represented by organic carbon-rich, smectite–kaolinite turbidites. Trace element data reveal significant enrichment in compatible and ferromagnesian elements consistent with a significant contribution from a basaltic crustal source. Although mixing of a basaltic source with granitic crust can account for specific geochemical relationships, mixing of these components cannot account for observed rare earth element (REE) patterns. REE data are best explained by mixing of basaltic detritus (e.g. Deccan Trap basalts of central India) with Precambrian tonalitic crust of the Indian subcontinent. A third group of carbonate-rich sediments (Group III), containing a low-latitude marine fauna, is characterized by a clastic component similar in composition to smectite–kaolinite turbidites. Although carbonate-rich sediments are superficially similar to Group II turbidites, geochemical data indicate a reduced contribution from basaltic crustal sources compared with smectite–kaolinite turbidites. A possible southern India/Sri Lankan provenance has been assigned to Group III turbidites on the basis of faunal content and geochemical composition, although insufficient information exists to substantiate this using geochemical data alone.

The distribution of lithofacies and provenance-sensitive geochemical signatures suggests that the relative contribution of Himalayan and Indian subcontinent sources to distal fan sedimentation varied with time. Controls on sediment supply include variations in uplift, weathering and erosion rates, eustatic sea-level changes, and switching of major distributary fan channels. Although a degree of correlation is observed between the occurrence of coarser-grained Himalayan-derived turbidites and relative low-stands, the relationship is patchy. Assuming that the rate of sediment supply from the Himalayas to the Bay of Bengal remained relatively constant, the most likely controls on distal fan sedimentation are thought to be related to an interplay between sea-level change and channel switching. As a consequence attempts to reconstruct major Himalayan tectonic and climatic events based on data obtained from a record of distal fan sedimentation may be unreliable due to the discontinuous nature of Himalayan sediment supply to distal fan sites.

The relationship between uplift and erosion of the Himalayan mountain chain and the growth of the Bay of Bengal deep-sea fan has been well documented on the basis of geophysical and sedimentological observations (Curray & Moore 1971; Emmel & Curray 1984; Curray 1994; Einsele *et al.* 1996). Mineralogical studies of Deep Sea Drilling Project (DSDP) Site 218 cores, shallow piston cores and dredge samples recovered from locations across the fan confirm the obvious importance of Himalayan erosion to fan sedimentation (Kolla & Biscaye 1973; Ingersoll & Suczek 1979; Bouquillon *et al.* 1989). Exceptions to a purely Himalayan provenance for Holocene and Pleistocene distal fan deposits have, however, been invoked by Goldberg & Griffin (1970), Kolla & Biscaye (1973) and Bouquillon *et al.* (1989) to account for the occurrence of smectite–kaolinite-rich sediments which have mineralogical affinities with basaltic and (or) high-grade metamorphic

CROWLEY, S. F., STOW, D. A. V. & CROUDACE, I. W. 1998. Mineralogy and geochemistry of Bay of Bengal deep-sea fan sediments, ODP Leg 116: evidence for an Indian subcontinent contribution to distal fan sedimentation. *In*: CRAMP, A., MACLEOD, C. J., LEE, S. V. & JONES, E. J. W. (eds) *Geological Evolution of Ocean Basins: Results from the Ocean Drilling Program*. Geological Society, London, Special Publications, **131**, 151–176.

crustal sources. Proposed sources for these sediments include the Deccan Trap basalts of central India and Precambrian high-grade metamorphic and igneous terrains exposed in central/southern India and Sri Lanka (Goldberg & Griffin 1970; Kolla & Biscaye 1973).

Investigation of Neogene sedimentation on the distal portion of the Bengal Fan by the Ocean Drilling Program (ODP Leg 116) resulted in the acquisition of a wide range of mineralogical and geochemical data (Cochran *et al.* 1989, 1990). Most of these data support the conclusion that quartz–mica–sodic plagioclase–chlorite–amphibole turbidites, which constitute much of the recovered core material, were derived from a source terrain dominated by rapid mechanical weathering and erosion of differentiated upper crustal rocks ([meta]sediments and granites) typical of the Himalayas (Bouquillon *et al.* 1990; Brass & Raman 1990; Yokoyama *et al.* 1990). In contrast, mineralogical and palaeomagnetic studies (Brass & Raman 1990; Sager & Hall 1990; Yokoyama *et al.* 1990; Aoki *et al.* 1991; Amano & Taira 1992) indicate that organic-rich (>1.0% total organic

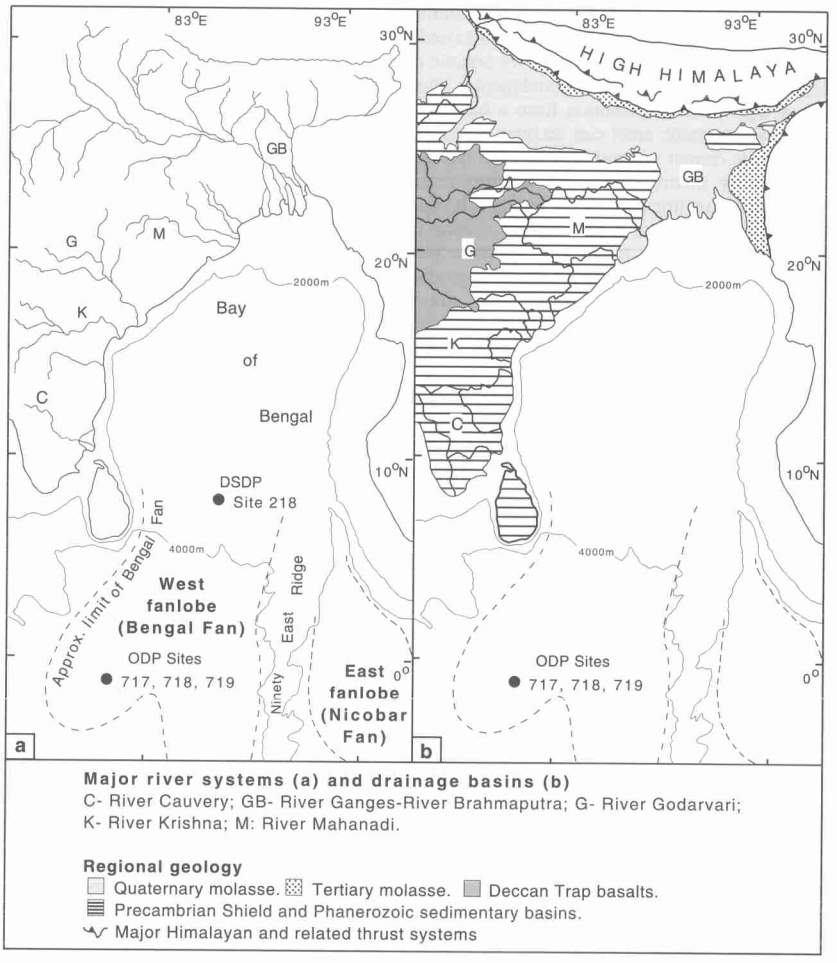

Fig. 1. Location map showing: (**a**) the geographical position of Leg 116 and major fluvial systems of the Himalayas and the Indian subcontinent; (**b**) regional geology and major drainage basin boundaries. The predominantly easterly directed drainage pattern of Indian subcontinent rivers is thought to have evolved in response to thermal uplift, underplating and rifting of the Indian shield during eruption of end-Cretaceous Deccan Trap flood basalts (Cox 1989). Continued uplift and erosion (Radhakrishna 1993) has resulted in considerable reduction in the geographical distribution of Deccan Trap basalts which originally covered much of the Indian subcontinent (Mahoney 1988).

carbon) sediments containing high concentrations of smectite and kaolinite were derived from the Indian subcontinent.

Bouquillon *et al.* (1990) and more recent publications (Derry & France-Lanord 1991; Derry *et al.* 1993; France-Lanord *et al.* 1993) have, however, drawn into question the importance of an Indian subcontinent contribution to distal fan sedimentation. They suggest, on the basis of similarities between the isotopic composition ($^{143}Nd/^{144}Nd$, $^{87}Sr/^{86}Sr$) of Himalayan crust and Neogene fan sediments, that virtually all distal fan turbidites were derived from the same Himalayan sources (High Himalaya Crystalline Series, with minor contributions from the Lesser Himalaya and the Tibetan Sedimentary Series). Differences in mineralogy (i.e. quartz–mica-rich *versus* smectite–kaolinite-rich sediments) are attributed to variations in the extent of chemical weathering (through either prolonged sediment storage of alluvium in floodplains or climate change) of Himalayan detritus prior to turbidite sedimentation. Importantly, France-Lanord *et al.* (1993) attribute differences in distal fan sediment mineralogy (and by implication the degree of chemical weathering) to the effects of major tectonic and climatic changes related to Himalayan uplift events. As a consequence, correct interpretation of the provenance of distal fan sediments and, in particular, the origin of smectite–kaolinite turbidites has important implications for understanding factors controlling: (1) tectonic and climatic change in sediment source terrains (specifically the Himalayas); (2) the evolution of sediment supply to the Bengal Fan; and (3) depositional sedimentary processes contributing to sediment accumulation in distal fan environments.

In this paper we address the question of sediment provenance on the basis of the mineralogy and trace element geochemistry of distal fan turbidites. These data are used in conjunction with published mineralogical and isotopic information to investigate the extent of chemical weathering of sediment source terrains, and identify the bulk crustal composition of source terrains supplying sediment to the distal fan. In addition, we utilize provenance-sensitive geochemical indicators to examine the temporal evolution of sediment supply to the distal fan with respect to Himalayan uplift and erosion, glacio-eustatic sea-level change, and behaviour of fan distributary channel systems.

Lithostratigraphy and sedimentology of distal Bengal Fan sediments

During ODP Leg 116 (Cochran *et al.* 1989) three closely spaced sites (717–719) were cored on the distal portion of the Bay of Bengal deep-sea fan (Fig. 1) resulting in the recovery of sediments ranging in age from Lower Miocene (*c.* 17.5 Ma) to Present (Fig. 2). All three sites penetrated similar

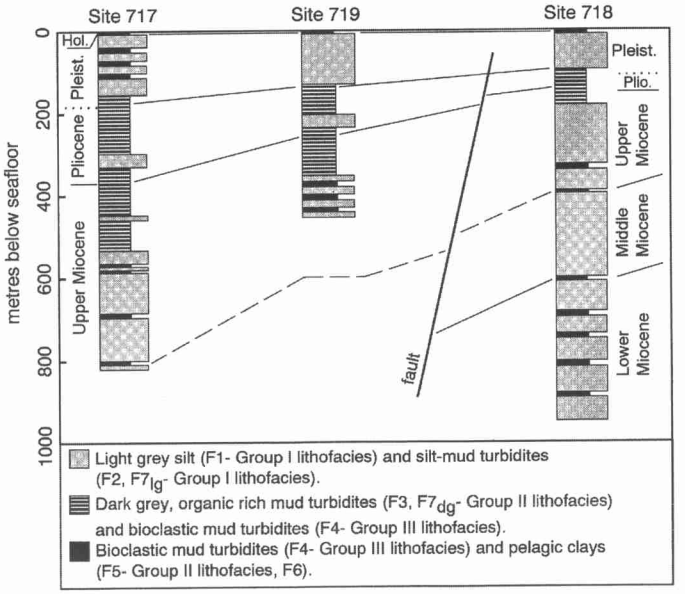

Fig. 2. Simplified lithostratigraphic logs for Sites 717, 718 and 719 (modified from Cochran *et al.* 1989; Cochran 1990).

Table 1. *Outline description of distal Bengal Fan lithofacies*

Facies	Lithology*	Range of mean grain sizes† (ϕ)	Mineralogy‡	Description
Silt, silt-mud turbidites (F1)	Litharenite–wacke–shale	4.32–7.51	Quartz, sodic plagioclase, K-feldspar, muscovite, biotite, chlorite, amphibole, calcite, dolomite	Sharp-based, normally graded, organic-poor (<0.5% TOC), light grey silt-to-mud turbidites. Rare bioturbation
Organic-poor mud turbidites (F2)	Shale–calcareous shale	6.31–7.84	Quartz, sodic plagioclase, K-feldspar, muscovite, biotite, chlorite, amphibole, calcite, dolomite	Sharp-based, normally graded, organic-poor (<0. 5% TOC), light grey mud turbidites. Sparse bioturbation
Organic-rich mud turbidites (F3)	Fe-shale–calcareous Fe shale	5.99–7.98	Quartz, plagioclase, smectite, kaolinite, illite, calcite, pyrite	Sharp-based, normally graded, organic-rich (>0.5% TOC), dark grey mud turbidites. Abundant authigenic pyrite. Localized bioturbation
Biogenic mud turbidites (F4)	Calcareous Fe-shale ($F4_{green}$)–limestone ($F4_{green}$, $F4_{white}$)	5.52–7.95	Calcite, aragonite, quartz, plagioclase, smectite, kaolinite, illite, pyrite	$F4_{green}$: sharp-based, normally graded, greenish-grey mud turbidites containing 10–50% biogenic carbonate. Localized bioturbation $F4_{white}$: sharp-based, normally graded, white turbidites containing >60% biogenic carbonate
Pelagic clays (F5)	Fe-shale ($F5_{red}$)–shale ($F5_{grey}$).	7.51–7.90	Quartz, plagioclase, smectite, kaolinite	Intensely bioturbated, organic-poor (<0. 5% TOC), red and light grey mud
Pelagic calcareous clays (F6)	Calcareous Fe-shale	7.25–7.43	Calcite, aragonite, quartz, plagioclase, smectite, kaolinite, illite, pyrite	Intensely bioturbated, white muds containing abundant (>30%) biogenic carbonate
Structureless muds . (F7)	Fe-shale ($F7_{dark\ grey}$)–shale ($F7_{light\ grey}$)	6.96–7.84	$F7_{dark\ grey}$: quartz, plagioclase, smectite, kaolinite, illite, calcite, pyrite. $F7_{light\ grey}$: quartz, sodic plagioclase, K-feldspar, muscovite, bioitite, chlorite, amphibole, calcite, dolomite	$F7_{dark\ grey}$: sharp-based (organic-rich, pyritic) 'hemiturbidites'. Localized intense bioturbation $F7_{light\ grey}$: sharp-based (organic-poor) mud 'hemiturbidites'. Localized intense bioturbation.

*Lithological classification scheme of Herron (1988)
†Data from Balson & Stow (1990)
‡Qualitative whole-rock X-ray diffraction. Minerals listed in order of estimated abundance

sedimentary sequences, but revealed significant differences in sediment thickness due to faulting and syndepositional intraplate deformation (Cochran 1990). The sediments were resolved into ten lithofacies (the following abbreviations are used: F1, F2, F3, $F4_{gr}$, $F4_{w}$, $F5_{r}$, $F5_{g}$, F6, $F7_{lg}$, $F7_{dg}$) during shipboard examination of core material. Detailed descriptions of these facies are reported in Stow *et al.* (1990). Grain-size characteristics, mineralogy and other features are summarized in Table 1.

In addition to primary depositional features, a variety of minor diagenetic processes were also recognized (Cochran *et al.* 1989; Aoki *et al.* 1991). These include: (1) the formation of authigenic pyrite (commonly associated with organic carbon-rich facies F3 and $F4_{gr}$) and a single calcite cemented horizon; (2) localized development of 'chemical fronts' formed by the relocation of redox-sensitive elements (Fe, Mn) in organic carbon-rich turbidites (F3); and (3) dissolution of siliceous and carbonate microfossils.

Sampling and analytical techniques

Forty-six samples were selected from cores recovered at ODP Sites 717 (0–740 metres below sea floor (mbsf); 0–8.9 Ma) and 718 (437–954 mbsf; 9.5–17.0 Ma) in order to provide data coverage through the available stratigraphy. All samples were dried at 105°C and crushed (<63 mm) in an agate mill. Qualitative mineralogical composition of each sample was determined by whole-rock X-ray diffraction (XRD). Analysis was performed on randomly orientated powders packed into aluminium mounts and scanned from 3 to 63°2θ.

Major element concentrations were determined by X-ray fluorescence (XRF) on fused glass discs (Harvey *et al.* 1973) at the University of Nottingham. The instrument was calibrated by analysing 12 international standard rocks (NIST and NIM standards) together with samples. Reference values for these standards were taken from Govindaraju (1989). Analytical precisions (see Harvey *et al.* 1973) are <1% for all major elements except Mg. Typical major element concentrations obtained from XRF analysis of international standards (G1, W1) run as 'unknowns' using this procedure are reported in Table 2. No attempt was made to remove water-soluble contaminants (notably salts precipitated from residual pore fluids) prior to analysis so that XRF-determined Na_2O data include Na present in both NaCl and sodic aluminosilicate phases. In order to correct Na_2O for salt contamination, soluble (non-silicate fraction) Na was measured by atomic absorption spectrophotometry following

Table 2. *Analyses of international standards by X-ray fluorescence (major elements) and instrumental neutron activation (trace elements)*

	G1*		W1*			JB1a*			
	XRFS analysis†	Certified value	XRFS analysis†	Certified value		INAA analysis	σ_{n-1} ($n = 6$)	Detection limit	Certified value
SiO_2	72.55	72.46	52.57	52.55	Co	39.4	0.2	0.3	39.5
Al_2O_3	14.40	14.23	14.83	14.99	Cr	418	4	3	415
TiO_2	0.27	0.25	1.06	1.07	Cs	1.1	0.1	0.2	1.2
$Fe_2O_3{}^T$	1.93	1.96	11.09	11.18	Hf	3.43	0.05	0.1	3.4
MgO	0.34	0.39	6.63	6.62	Rb	42	2	8	41
CaO	1.32	1.38	10.94	10.94	Sc	29.14	0.10	0.06	29
Na_2O	3.30	3.33	2.12	2.13	Ta	1.99	0.03	0.10	2.0
K_2O	5.49	5.48	0.66	0.64	Th	8.82	0.09	0.20	8.8
MnO	0.03	0.03	0.17	0.17	U	1.60	0.11	0.50	1.6
P_2O_5	0.08	0.09	0.14	0.14	La	37.8	0.9	0.3	38
					Ce	66.7	0.8	1.0	67
					Nd	25	1	3	24
					Sm	5.18	0.10	0.05	5.2
					Eu	1.49	0.03	0.05	1.5
					Tb	0.71	0.02	0.05	0.70
					Tm	0.34	0.01	0.15	0.34
					Yb	2.05	0.07	0.10	2.0
					Lu	0.33	0.01	0.10	0.33

*Certified values from Potts *et al.* (1992)
†Data from Harvey *et al.* (1973)

dissolution in deionized water (McLennan *et al.* 1990) and the data reported as Na_2O^* (XRF Na_2O – water-soluble Na_2O). Estimates of relative precision and accuracy based on analysis of artificial mixtures of silica sand and reagent grade NaCl were <5% for Na contents ranging between 0.5 and 2 wt%.

Total organic carbon (TOC), inorganic carbon (TIC) and total sulphur (TS) contents were measured using a Carlo Erba C-H-N-S element analyser at the University of Southampton (TOC, TIC) and the University of Leeds (TS). Detection limits are 0.01 wt% and 0.005 wt% for carbon and sulphur respectively, with relative precisions and accuracies of <5% for both techniques at concentrations above 1 wt%.

Trace element concentrations were determined by instrumental neutron activation analysis (INAA). Samples were irradiated for 24 h under a neutron flux of 1×10^{12} cm^{-2} s^{-1}. Counting was carried out at the University of Southampton by collecting spectra simultaneously using a Canberra Industries 16% P-type HPGe and a Canberra Industries planar Ge spectrometer at 7 and 30 days after irradiation. Data were processed using Canberra APOGEE software. Element concentrations were obtained following corrections for flux variation and calibrated by using international reference samples NIM-G and BHVO. Detection limits, estimates of analytical reproducibility (σ_{n-1}) based on replicate analysis of the JB1a standard, and certified values for JB1a (Potts *et al.* 1992) are reported in Table 2.

Mineralogical and geochemical results

In order to simplify the presentation of analytical results (a tabulation of all data reported in this paper is provided in the Appendix), the range of individual lithofacies has been reduced to the following three groups based on general facies associations (see Stow *et al.* 1990), similarities in mineralogy, major element geochemistry and principal component analysis of major element data (Fig. 3): Group I. – F1, F2, $F7_{lg}$; Group II. – F3, $F5_r$, $F7_{dg}$; and Group III. – $F4_{gr}$. Variations in the composition of individual facies are, however, discussed where appropriate.

Mineralogy

Qualitative whole-rock XRD analysis of distal fan turbidites largely confirms the results of more detailed studies conducted by Bouquillon *et al.* (1990) and Brass & Raman (1990), although data obtained during this investigation provide complementary information on the mineralogy of these sediments.

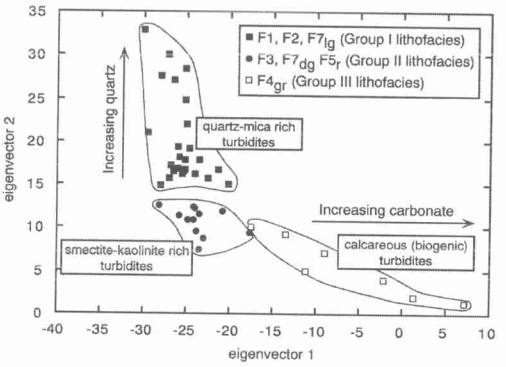

Fig. 3. Principal component plot for distal Bengal Fan sediments. Eigenvectors are calculated from anhydrous (LOI-free), normalized major element data (MnO and P_2O_5 were not included due to the low concentration of these oxides). Eigenvectors, eigenvalues and variance proportions for the first three principal components are listed below. Large eigenvalues for the first two principal components (V1 and V2) account for a significant proportion of the total variability of the data. V1 effectively discriminates calcareous from non-calcareous sediments, while V2 discriminates between $Fe_2O_3^T$–Al_2O_3-rich (smectite–kaolinite) and SiO_2–K_2O–Na_2O^*-rich (quartz–mica–feldspathic) sediments. Fields outlining the three lithofacies groupings are hand-drawn. Na_2O^* is Na_2O present in silicate minerals only (see text for details).

Eigenvectors	V1	V2	V3
SiO_2	–0.313	0.461	0.269
Al_2O_3	–0.442	–0.222	–0.148
TiO_2	–0.291	–0.476	0.272
$Fe_2O_3^T$	–0.255	–0.543	0.135
MgO	–0.336	–0.019	–0.613
CaO	0.474	–0.047	–0.196
K_2O	–0.354	0.301	–0.444
Na_2O^*	–0.308	0.351	0.449
Eigenvalue	4.088	2.188	1.287
Variance proportion (%)	51.1	27.3	16.1

Group I. Samples of Group I turbidites are characterized by the occurrence of mica (muscovite, biotite), chlorite, amphibole, sodic plagioclase and potassium feldspar. Quartz and variable (but generally minor) quantities of calcite and dolomite occur in all samples. Variations in mineralogical abundances are most probably related to the grain size of sediment reaching the distal portion of the fan and the unmixing of density current components during deposition. As a consequence the proportion of quartz and feldspar (as indicated by relative peak XRD heights) increases

relative to sheet silicate minerals, calcite and dolomite with increasing sediment grain size (estimated from visual inspection of hand specimens).

Group II. The mineralogy of Group II turbidites differs considerably from samples of Group I. Diffraction patterns reveal the occurrence of variable amounts of smectite and (or) mixed-layer clays, kaolinite, illite and pyrite. Quartz and feldspar occur in all samples, but are present in reduced concentrations compared to Group I due to the higher clay mineral content of Group II sediments. Calcite and dolomite are present in the majority of samples, although carbonates rarely contribute significantly to bulk mineralogy.

Group III. Group III turbidites contain large concentrations of biogenic carbonate and are characterized by the occurrence of calcite and aragonite. Associated silicate phases include quartz, plagioclase, smectite, kaolinite and illite/mica. Minor quantities of dolomite and pyrite are present in virtually all cases. Importantly, those $F4_{gr}$ samples containing relatively low carbonate abundances reveal whole-rock XRD patterns similar to those recorded from Group II turbidites.

Major element geochemistry

Samples recovered from Leg 116 cores are primarily composed of silt and clay grade sediment (Balson & Stow 1990) and, as an alternative to standard petrographic schemes, have been classified using SandClass (Herron 1988, see Fig. 4). The scheme effectively separates samples on the basis of lithic to feldspar content ($Fe_2O_3{}^T/K_2O$), the proportion of quartz to sheet silicate minerals (SiO_2/Al_2O_3) and carbonate abundance (CaO). Data plotted using SandClass (Fig. 4) reveal three dominant sediment populations corresponding to the facies grouping recognized on the basis of lithological characteristics, XRD mineralogy and principal component analysis of major element data (see Fig. 3).

Group I. Group I turbidites are characterized by a linear array of compositions ranging from litharenites to shales (three calcareous Group I samples also plot on this trend). This array is attributed to the progressive hydraulic separation (unmixing) of quartz and feldspar from sheet silicate minerals during deposition of turbidites from sediment density currents. Compositional relationships expressed in terms of a correlation matrix (Table 3a) show that TiO_2, $Fe_2O_3{}^T$, MgO and K_2O are positively correlated with Al_2O_3 and negatively correlated with SiO_2. Interelement relationships are consistent with the occurrence of essentially two 'independently differentiable components' (Argast & Donnelly 1987). This results in the concentration of TiO_2, $Fe_2O_3{}^T$, MgO and K_2O in sheet silicates (chlorite, biotite, muscovite) and the separation of SiO_2 (quartz) from other elements through depositional processes. Na_2O^* is negatively correlated with all major elements apart from SiO_2 and indicates that sodium probably occurs largely in sodic plagioclase. In contrast, CaO is only weakly correlated with other elements suggesting that Ca is distributed between a variety of phases (e.g. calcite, dolomite, apatite, plagioclase). TOC contents are

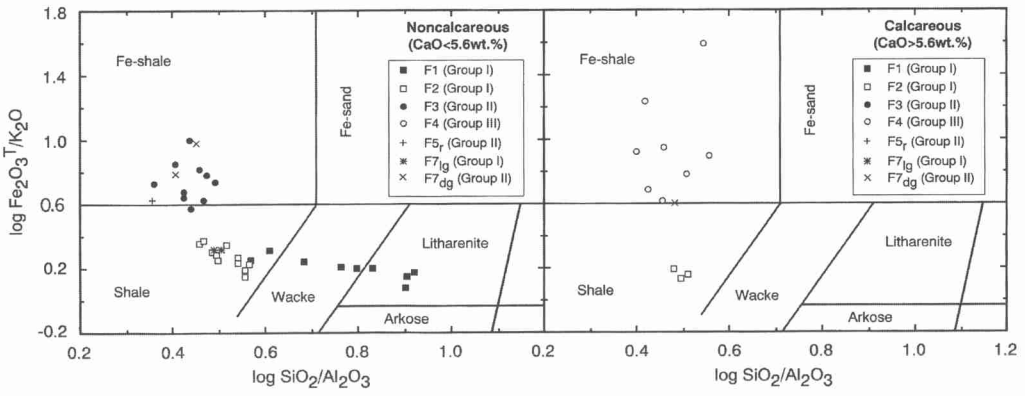

Fig. 4. Geochemical classification of distal Bengal Fan sediments using SandClass (Herron 1988). Brief lithofacies descriptions are provided in Table 1. Lithofacies F4 are characterized by high CaO contents (>5.6 wt% CaO) compared to most other fan deposits and define a third distinct geochemical grouping comprising calcareous sediments rich in biogenic carbonate.

Table 3. *Pearson product–moment correlation matrix*

	SiO_2	Al_2O_3	TiO_2	$Fe_2O_3{}^T$	MgO	CaO	K_2O	Na_2O*	MnO	P_2O_5	S
(a) Group I lithofacies (n = 25)											
SiO_2	–										
Al_2O_3	–0.892	–									
TiO_2	–0.791	0.841	–								
$Fe_2O_3{}^T$	–0.777	0.931	0.854	–							
MgO	–0.962	0.801	0.717	0.662	–						
CaO	–0.206	–0.244	–0.197	–0.418	0.323	–					
K_2O	–0.887	0.908	0.666	0.807	0.832	–0.042	–				
Na_2O*	0.720	–0.532	–0.432	–0.432	–0.710	–0.398	–0.667	–			
MnO	–0.596	0.649	0.604	0.604	0.474	–0.129	0.480	–0.240	–		
P_2O_5	–0.566	0.480	0.329	0.329	0.617	0.214	0.368	–0.282	0.245	–	
S	–0.243	0.367	0.373	0.599	0.141	–0.401	0.342	–0.105	0.192	–0.084	–
(b) Group II lithofacies (n = 14)											
SiO_2	–										
Al_2O_3	0.187	–									
TiO_2	0.219	0.441	–								
$Fe_2O_3{}^T$	–0.135	–0.256	0.347	–							
MgO	0.671	–0.173	–0.271	–0.152	–						
CaO	–0.566	–0.486	–0.689	–0.484	–0.240	–					
K_2O	0.347	–0.144	–0.589	–0.562	0.631	0.274	–				
Na_2O*	0.161	0.166	0.618	0.477	–0.388	–0.576	–0.595	–			
MnO	–0.119	0.088	0.234	0.079	0.169	–0.138	0.170	–0.055	–		
P_2O_5	–0.545	–0.338	–0.454	–0.398	–0.191	0.718	0.159	–0.465	–0.231	–	
†S	–0.449	–0.395	0.205	0.843	–0.249	–0.200	–0.414	0.375	0.290	–0.55	–
(c) Group III lithofacies (n = 7)											
SiO_2	–										
Al_2O_3	0.965	–									
TiO_2	0.986	0.941	–								
$Fe_2O_3{}^T$	0.861	0.932	0.860	–							
MgO	0.843	0.944	0.835	0.922	–						
CaO	–0.966	–0.996	–0.949	–0.937	–0.945	–					
K_2O	0.969	0.960	0.933	0.811	0.863	–0.946	–				
Na_2O*	0.964	0.920	0.927	0.746	0.798	–0.913	0.984	–			
MnO	–0.844	–0.871	–0.863	–0.783	–0.866	0.898	–0.798	–0.778	–		
P_2O_5	–0.802	–0.701	–0.774	–0.530	–0.575	0.727	–0.779	–0.873	0.663	–	
S	–0.283	–0.095	–0.292	0.000	0.089	0.071	–0.300	–0.370	–0.182	0.379	–

†S: Inter-element correlations calculated using F3 and $F7_{dg}$ data only

uniformily low and rarely exceed 0.5 wt%. Highest TOC contents are associated with fine-grained lithofacies (F2, $F7_{lg}$) reflecting the hydraulic separation of organic matter from coarser-grained components during deposition. Sulphur concentrations are similarly low (generally <0.2 wt%) and indicate the presence of only minor quantities of detrital sulphide and sulphate minerals (Fig. 5).

Group II. Smectite–kaolinite turbidites form a broad cluster of data which plot away from the trend defined by Group I samples and fall predominantly within the Fe-shale field of SandClass (Fig. 4). Fewer significant interelement relationships are defined by linear correlations (Table 3b) due to the absence of differentiable components and wide variations in the geochemistry of detrital phases present in these sediments (Aoki *et al.* 1991). Weak positive correlations between SiO_2, MgO and K_2O may indicate an interdependent relationship between quartz and mica, while negative correlations between Al_2O_3 and other major elements possibly reflect the importance of kaolinite in these samples. In comparison to Group I lithofacies, Group II turbidites are generally rich (>0.5 wt%) in sulphur ($F5_r$ is an exception) as the result of the formation of diagenetic pyrite (Cochran *et al.* 1989). The fact that the S–$Fe_2O_3{}^T$ correlation for Group II sediments closely parallels the stoichiometric pyrite line (Fig. 5) indicates that a proportion of Fe present in the majority of samples is contained within pyrite. Intersection of

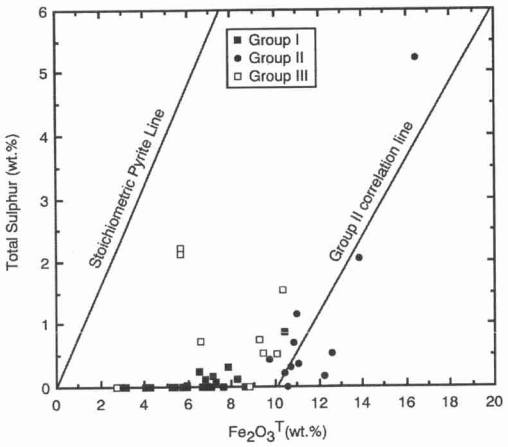

Fig. 5. Total sulphur–$Fe_2O_3^T$ diagram showing variations in Fe content of fan sediments with respect to S. The low S contents of Group I turbidites are consistent with low detrital/authigenic sulphate and sulphide abundances. In contrast, the high Fe concentration of Group II turbidites are in part dependent on pyrite content as indicated by the parallel trends of the Group II S–$Fe_2O_3^T$ correlation and the stoichiometric pyrite lines.

the regression with the $Fe_2O_3^T$ axis, however, shows that approximately 10 wt% $Fe_2O_3^T$ occurs in other (? detrital) phases. Although variable, the TOC content of Group II turbidites typically exceeds 1 wt% and provides a further important geochemical contrast with Group I sediments.

Group III. Carbonate-rich lithofacies are characterized by high CaO (7–40 wt%) and $Fe_2O_3^T/K_2O$, and low SiO_2/Al_2O_3. Group III turbidites consequently range from calcareous Fe-shales to limestones (Fig. 4). Although samples are variably diluted by biogenic carbonate, SandClass shows that the siliciclastic portions of these sediments have compositional affinities with Group II lithofacies, and this relationship is further supported by an overall similarity in major element geochemistry of Group III sediments when estimated on a CaO-free basis. TOC contents of carbonate-rich sediments are variable and occasionally higher than other distal fan facies. Although TOC data might possibly reflect an increased marine organic input associated with high biogenic carbonate contents, Rock-Eval pyrolysis data (Cochran *et al.* 1989) show that organic matter present in Group III sediments is dominated by terrestrial sources. TOC may be related to either (or both) high initial organic matter contents in source sediments or concentration of detrital organic matter by hydraulic factors during deposition. Sulphur is only weakly correlated with other elements (Table 3c) and this indicates that S is probably present in a variety of sulphate and sulphide phases.

Trace element geochemistry

In order to rationalize variability in the trace element geochemistry of fan sediments, data from different lithofacies are compared by using

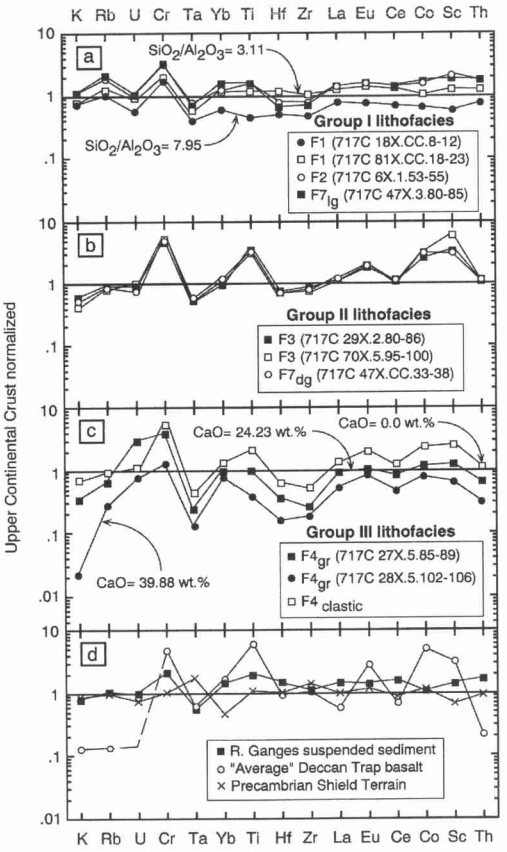

Fig. 6. Upper Continental Crust normalized trace element patterns (elements are ordered from left to right in terms of increasing ocean residence times). (**a**) Group I lithofacies. (**b**) Group II lithofacies. (**c**) Group III lithofacies (see text for details of methods used to estimate the composition of $F4_{clastic}$ [0. 0 wt% CaO]). (**d**) River Ganges suspended sediment (data from Martin & Meybeck 1979), 'average' Deccan Trap basalts (Ambenali, Mahabaleshwar, Panhala and Poladpur Formations (Lightfoot 1985)), Precambrian shield terrain (present-day Canadian Shield surface composition estimate of Shaw *et al.* (1986)). Upper Continental Crust values from Taylor & McLennan (1985). Zr concentrations in Bengal fan sediments are estimated assuming Zr = Hf × 39 (Condie 1991).

multielement plots (Figs 6 and 7) normalized to average Upper Continental Crust (Taylor & McLennan 1985) and chondrite (Briqueu *et al.* 1984).

Group I. Normalized trace element data (Fig. 6a) reveal relatively flat profiles corresponding to a bulk composition close to Upper Continental Crust. Chondrite-normalized rare earth element (REE) patterns (Figs 7a and 8) are similar to most Phanerozoic clastic sediments (Taylor & McLennan 1985; McLennan 1989) and are distinguished by light rare earth element (LREE) enrichment (La_N/Yb_N >7.5, La_N/Sm_N >2.0), relatively flat heavy rare earth element (HREE) (Gd_N/Yb_N<2.0) and depleted Eu-anomalies (Eu/Eu* <0.85). Although the pattern of trace element and rare earth element behaviour between individual lithofacies is similar, total trace element and REE abundances decrease systematically with increasing SiO_2/Al_2O_3, consistent with the concentration of these elements in the fine-grained, sheet silicate-rich fraction of turbidite sediments (Taylor & McLennan 1985; McLennan *et al.* 1990).

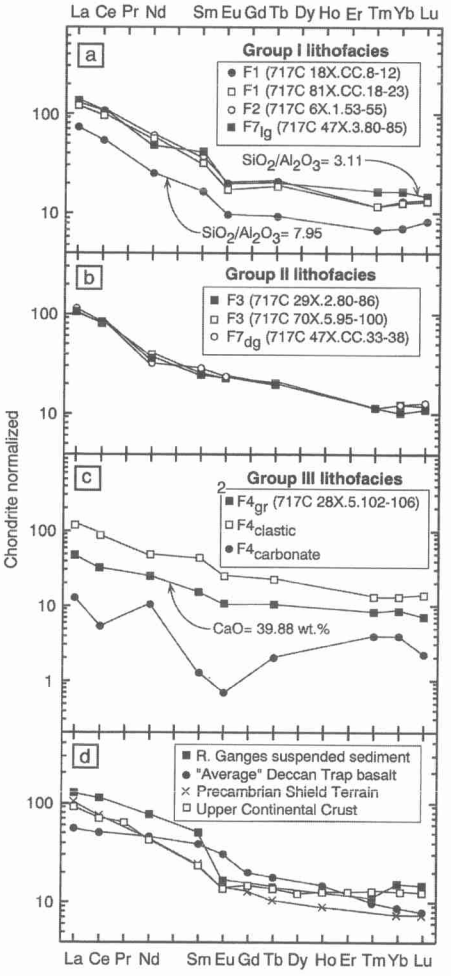

Fig. 7. Chondrite-normalized REE patterns. (**a**) Group I lithofacies. (**b**) Group II lithofacies. (**c**) Group III lithofacies (see text for details of methods used to estimate the REE composition of $F4_{clastic}$ and $F4_{carbonate}$). (**d**) River Ganges suspended sediment, Precambrian shield terrain and 'Average' Deccan Trap basalts and Upper Continental Crust (see Fig. 6 for details of data sources). Chondrite normalization values from Briqueu *et al.* (1984).

Group II. In contrast to Group I turbidites, the majority of Group II samples (Figs 6b and 7b) are characterized by Co, Cr, Sc, Ti, Eu (Eu/Eu*>0.85) enrichment and K, Rb, Th depletion when compared to Upper Continental Crust. This is indicative of a higher mafic content than is typical of many Phanerozoic sediments (Taylor & McLennan 1985; McLennan 1989) and sedimentary successions deposited in a passive margin tectonic environment (McLennan *et al.* 1990). Group II sediments, however, exhibit LREE (La_N/Yb_N >7.5, La_N/Sm_N >2.0) patterns similar to those displayed by Group I turbidites (Fig. 8) and in this respect are similar in composition to Upper Continental Crust and average Phanerozoic clastic sediments (Taylor & McLennan 1985; McLennan 1989).

Group III. Carbonate-rich lithofacies exhibit differing total trace element concentrations and normalized patterns (Figs 6c and 7c) as a result of variations in the abundance of trace element-depleted biogenic carbonate. Estimates of the trace element and REE composition of clastic and carbonate end-members for $F4_{gr}$ samples, using a least-squares fit of trace element data against CaO (assuming bimodal mixing between terriginous (0 wt% CaO) and carbonate (56 wt% CaO) sediment), produce distinctly different geochemical signatures (Figs 6c and 7c). The resultant pattern for the terrigenous component reveals compositional features similar to those displayed by Group II sediments, although the depleted Eu/Eu* (Eu/Eu* = 0.72) is more consistent with Eu anomalies observed in Group I turbidites (Fig. 8). In contrast, the carbonate end-member is characterized by low total trace element concentrations and exhibits REE compositional features (depleted Ce anomaly, HREE enrichment) similar to those of marine bioclasts (cf. Elderfield *et al* 1981).

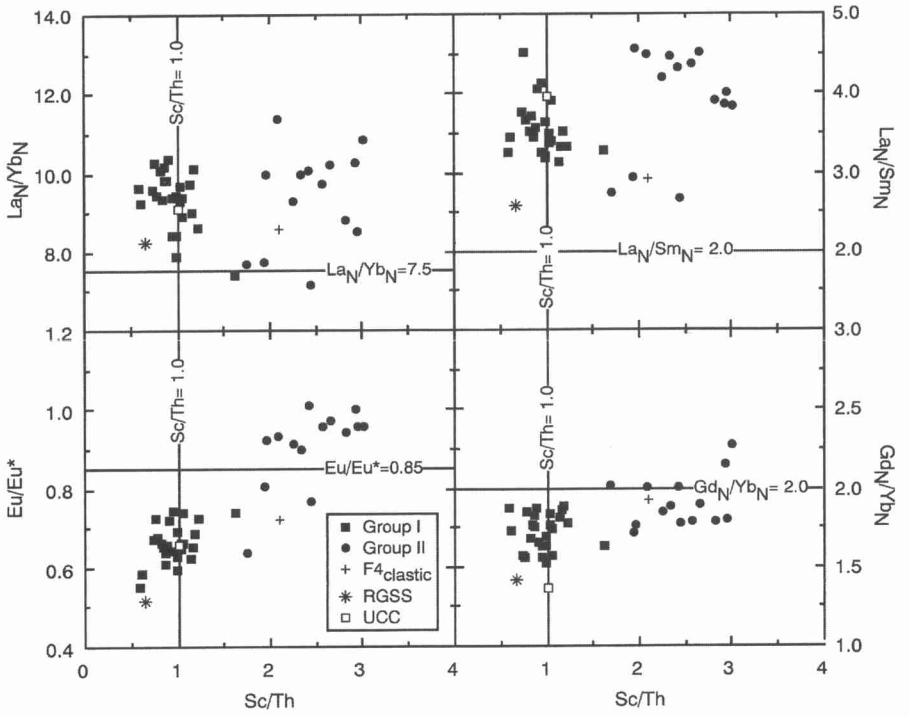

Fig. 8. La_N/Yb_N, La_N/Sm_N, Eu/Eu*, Gd_N/Yb_N–Sc/Th diagrams showing the distribution of distal fan sediments, River Ganges suspended sediment (RGSS; Martin & Maybeck 1979) and Upper Continental Crust (UCC; Taylor & McLennan 1985). Gd_N estimated assuming $Gd_N = (Sm_N x Tb_N^2)^{1/3}$, $Eu/Eu^* = Eu_N/(Sm_N x Gd_N)^{1/2}$. All published data recalculated using the chondrite values of Briqueu *et al.* (1984).

Discussion

Source terrain weathering: mineralogical and geochemical evidence

Estimates of the extent of source terrain weathering based on the relative behaviour of specific groups of elements such as the alkali metals, alkaline earths and Th–U in resultant sediments have proven to provide reliable indicators of chemical weathering intensity (Nesbitt *et al.* 1980; Nesbitt & Young 1982, 1984; McLennan *et al.* 1990, 1993). For alkali and alkaline earth elements, Nesbitt *et al.* (1980) have shown that cations with large ionic radii (Rb, Cs) are generally fixed within the products of weathering profiles by formation of new phases and adsorption onto exchange sites of clay minerals, whereas cations with smaller radii (Na, Ca, Sr) are selectively leached during weathering and remain in solution. Similarly, differences in the solubility of U and Th during weathering offer a further means of assessing and comparing the degree of chemical weathering (McLennan *et al.* 1993) as a result of the increased solubility and loss of U in oxidizing environments and the retention of Th (leading to increased Th/U) with progressive chemical weathering. The relative response of alkali and alkaline earth elements can be used as a guide to the extent of chemical weathering (Nesbitt & Young 1982) and this is expressed quantitatively as a Chemical Index of Alteration (CIA; see Fig. 9). Chemical weathering trends may also be monitored using the A–C*N*–K diagrams (see Fig. 10) of Nesbitt & Young (1989). These diagrams provide a convenient way of comparing the extent of source terrain weathering, assessing chemical weathering pathways and evaluating the bulk lithological and geochemical composition of source terrains.

Regardless of crustal source, differences in the mineralogy of distal fan sediments, particularly with respect to clay mineralogy and feldspar content, suggest a considerable variation in the relative intensity of chemical weathering prior to deposition of each of the lithofacies groupings. In general terms the high plagioclase feldspar, mica (including biotite), chlorite and amphibole content of Group I turbidites is consistent with rapid

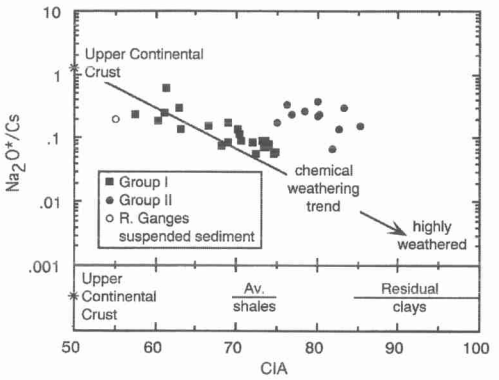

Fig. 9. Na_2O^*/Cs–CIA (Chemical Index of Alteration; Nesbitt & Young 1982) diagram for distal fan sediments. $CIA = Al_2O_3/(Al_2O_3 + CaO^* + Na_2O^* + K_2O) \times 100$, where: oxides are in molecular proportions; CaO^* is the CaO content minus CaO present in carbonates and apatite; Na_2O^* is Na_2O present in silicate minerals only (see text for details). XRD analysis shows that calcite and dolomite are the main carbonate phases present in Group I and Group II turbidites. CaO^* was calculated assuming that inorganic carbon (TIC) is divided equally between calcite and dolomite. Although CaO^* values are calculated with greater uncertainty, this compromise does not significantly affect interpretation. Values for Group III turbidites are not included due to high residual CaO^* contents after correction for the presence of carbonate minerals and apatite. River Ganges suspended sediment data from Martin & Meybeck (1979). Values for Upper Continental Crust, shales and residual clays are from Taylor & McLennan (1985).

erosion of sediments derived from a source region(s) dominated by mechanical weathering processes (Curtis 1990). In contrast, Group II and Group III turbidites contain significantly smaller quantities of feldspar and are characterized by high concentrations of smectite and kaolinite reflecting relatively intense chemical weathering of source terrains (Nesbitt & Young 1984; Curtis 1990).

Despite problems caused by the presence of both detrital (calcite, dolomite) and biogenic carbonates (calcite, aragonite), distal fan sediment data reveal good agreement between the extent of chemical weathering based on mineralogical observations and estimates of relative chemical weathering intensity using CIA (Fig. 9). Importantly, the separate trends defined by Group I and Group II turbidites in Na_2O^*/Cs–CIA space (Fig. 9) imply progressive chemical weathering of sources terrains with differing bulk compositions and this is supported by the pattern of geochemical behaviour observed from data plotted on an A-C*N*-K diagram (Fig. 10). Here the distribution of Group I turbidites corresponds with that expected for progressive chemical weathering of rocks with a bulk composition similar to granite (although the progressive weathering trend displayed by these data may also reflect the effects of grain-size separation as K_2O-rich sheet silicates are partitioned into fine-grained lithofacies during deposition). In comparison, Group II turbidite data fall along a trend which is consistent with weathering of a source terrain with a bulk composition similar to tonalite–granodiorite (Fig. 10).

Similar conclusions regarding compositional differences in source terrain geochemistry may be drawn from U–Th data (Fig. 11). Although most samples exhibit Th/U ratios greater than upper crustal values, samples from Group I turbidites are characterized by higher Th/U ratios than those of Group II despite mineralogical and other geochemical evidence which suggests that Group I sediments are less intensely weathered. Because diagenetic processes may modify Th/U ratios it is not immediately certain whether authigenic U enrichment or differences in the composition of sediment source terrains are responsible for observed geochemical differences. Estimates of apparent authigenic U content (Myers & Wignall 1987) and U/Th ratios, however, indicate that both Group I and Group II turbidites were deposited under relatively oxic environmental conditions and that no significant diagenetic enrichment of U has occurred (see Jones & Manning (1994) for details). As a consequence the behaviour of Th–U in distal fan sediments is consistent with alkali and alkaline earth element data in supporting different bulk crustal compositions for the source terrains of Group I and Group II turbidites.

Crustal sources and sediment provenance: trace element geochemistry

Although trace elements may be partitioned by chemical weathering processes (Nesbitt 1979; Nesbitt *et al.* 1980; Marsh 1991), a number of studies (Taylor & McLennan 1985; McLennan 1989; McLennan *et al.* 1990, 1993; Condie 1991; Cullers 1994) have shown that certain elements with low solubilities do not remain in solution following weathering and are essentially recycled quantitatively as part of the detrital sediment load during erosion and transport. Consequently, although absolute abundances may change relative to source rock geochemistry as the result of the loss of highly soluble components (Na, Ca, Mg, Sr), elements such as Co, Cr, Hf, Sc, Th, REE are generally transported in ratios consistent with ratios present in primary crustal sources and may be used to infer the geochemical characteristics of sediment

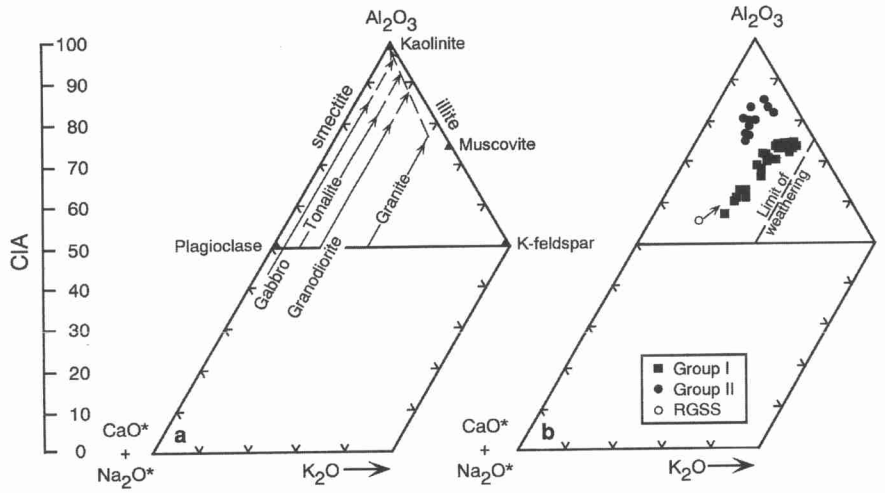

Fig. 10. A–C*N*–K diagrams (Nesbitt & Young 1989) illustrating: (a) ideal chemical weathering trends for common rock types (Nesbitt & Young 1989); and (b) distal fan sediments. Full arrows indicate predicted weathering paths; dashed arrows are extensions of these pathways to highly weathered, residual soils. River Ganges suspended sediment (RGSS) data are from Martin & Maybeck (1979). Note the relatively high CaO content (4.1 wt%) of RGSS has not been corrected for CaO present in carbonate minerals or apatite resulting in displacement towards CaO* (arrow indicates likely locus of RGSS). All values are in molar proportions (see Fig. 9 and Nesbitt & Young (1982) for details of CaO* calculations). Na_2O^* is Na_2O present in silicate minerals only (see text for details).

source terrains and to assess the relative contribution of geochemically distinct crustal sources (Taylor & McLennan 1985; Condie & Wronkiewicz 1990). In addition, provenance-sensitive geochemical signatures based on a broad range of elements normalized against representative bulk crustal averages such as Upper Continental Crust (Taylor & McLennan 1985) can be used to discriminate between sediments derived from different source terrains and to identify the tectonic setting of sedimentary basins (McLennan *et al.* 1990, 1993). Both approaches are used to characterize the provenance of each of the major facies groups.

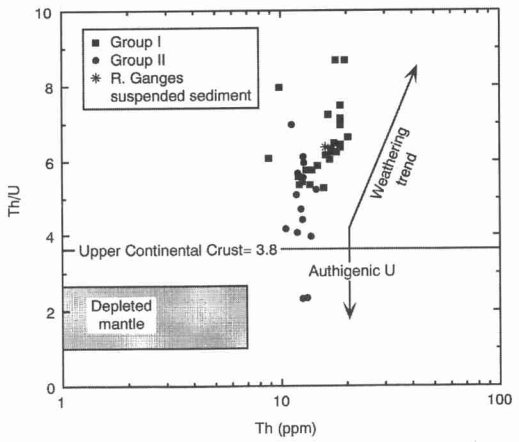

Fig. 11. Plot of Th/U–Th. Note that Group II samples have Th/U ratios similar to or less than those observed for Group I turbidites. River Ganges suspended sediment data are from Martin & Meybeck (1979). Upper Continental Crust, authigenic enrichment trend, weathering trend and depleted mantle compositions are from Taylor & McLennan (1985) and McLennan *et al.* (1993).

Group I. The relatively flat Upper Continental Crust normalized trace element signatures of Group I turbidites (Fig. 6a) indicate that these sediments are derived from a recycled orogenic (passive margin) provenance characterized by upper crustal rocks similar in bulk composition to granite (Taylor & McLennan 1985; McLennan *et al.* 1990, 1993). Specific features such as high SiO_2/Al_2O_3, marked depleted Eu anomalies (Eu/Eu* *c.* 0.65), LREE (La_N/Yb_N>7.5) and large ion lithophile element (Cs, K, Rb, Th) enrichment, and relative depletion in compatible and mafic elements (Co, Cr, Sc, Ti) are all consistent with a source terrain dominated by rocks of granitic composition. Together with the quartz–sodic plagioclase–mica–chlorite–amphibole mineralogy, the geochemical data are compatible with sediments sourced by mixed (meta)sedimentary–granitic lithologies similar to those present within the Himalayan mountain belt

(Bouquillon *et al.* 1990; Yokoyama *et al.* 1990; France-Lanord *et al.* 1993).

Similarities between the bulk geochemistry of the Himalayas and distal fan sediments are further strengthened by general comparison of Group I lithofacies with modern River Ganges suspended sediment (Figs 6d, 7d and 8). However, Group I turbidites are generally enriched in compatible elements (Co/Th, Cr/Th, Sc/Th) and have higher Eu/Eu* when compared with River Ganges suspended sediment (Figs 7 and 12). These features may indicate a greater contribution of basaltic crust to the Ganges–Brahamaputra sediment dispersal system during Neogene fan deposition compared to modern sediment supply (Figs 13 and 14).

Group II. In contrast to the bulk upper crustal provenance inferred from the geochemistry of Group I turbidites, Group II lithofacies exhibit mineralogical (high smectite content) and geochemical characteristics (Co, Cr, Fe, Ti, Sc enrichment; K, Rb, Th depletion; Sc/Th>1; Eu/Eu*>0.85; Figs 6b, 7b and 8) which suggest an important detrital input from basaltic crustal sources (Taylor & McLennan 1985; McLennan *et al.* 1990, 1993). This enrichment is shown clearly on Th–Hf–Co, La–Th–Sc and Co/Th–La/Sc diagrams (Figs 12 and 13) where individual samples plot towards basaltic compositions. Group II turbidites, however, reveal features (La_N/Yb_N>7.5, Gd_N/Yb_N>2.0, low Sc/Th) and display mixing trends (Figs 12 and 13) which are incompatible with a purely basaltic sediment provenance such as the Deccan Trap basalts of central India (see Fig. 1), and this necessitates mixing of basaltic detritus with sediment derived from source lithologies characterized by LREE enrichment, HREE and compatible element depletion, and Eu/Eu*>0.85.

Although data clearly satisfy mixing between basaltic and grantic crustal sources for certain trace elements (Fig. 13), bimodal mixing of these components is unable to account for the high Eu/Eu* values which characterize Group II turbidites (see Fig. 8). An alternative bulk crustal source to granite which meets the requirements of LREE enrichment, HREE and compatible element depletion, and Eu/Eu*>0.85 may be found by substituting tonalite–trondhjemite–granodiorite (TTG; Condie 1993) for granite in mixing models (see Fig. 14 for details). Major crustal reservoirs with a bulk composition similar to TTG are most likely to occur within Precambrian Shield terrains where tonalitic rocks constitute a significant proportion of crustal volume (Condie 1993). Archaean rocks of the Indian Shield, in particular, provide a potentially important reservoir of tonalitic crust (Radhakrishna & Naqvi 1986;

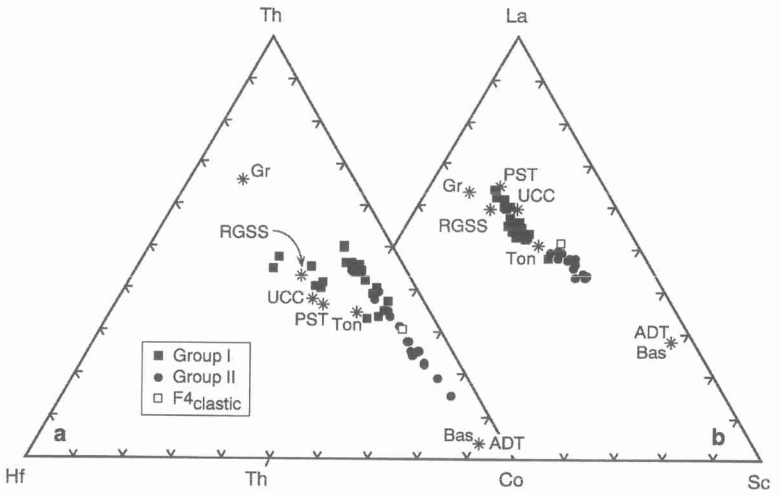

Fig. 12. Ternary diagrams (**a**) Th–Hf–Co and (**b**) La–Th–Sc showing the distribution of distal Bengal Fan sediments. Linear arrays indicate bimodal mixing. Displacement of some Group I lithofacies data towards the Hf apex implies a higher zircon content in these samples. A positive covariant relationship ($r = 0.673$) between Hf and SiO_2/Al_2O_3 suggests that high Hf contents are related to grain size partitioning and the concentration of zircon in coarser-grained turbidite deposits as opposed to recycling of old (meta)sedimentary rocks (McLennan *et al.* 1993). Data sources for River Ganges suspended sediment (RGSS), Precambrian shield terrain (PST), 'average' Deccan Traps and Upper Continental Crust (UCC) are given in Fig. 6. Gr, Phanerozoic granite; Ton, Phanerozoic tonalite–trondhjemite–granodiorite; Bas, Phanerozic basalt are taken from Condie (1993).

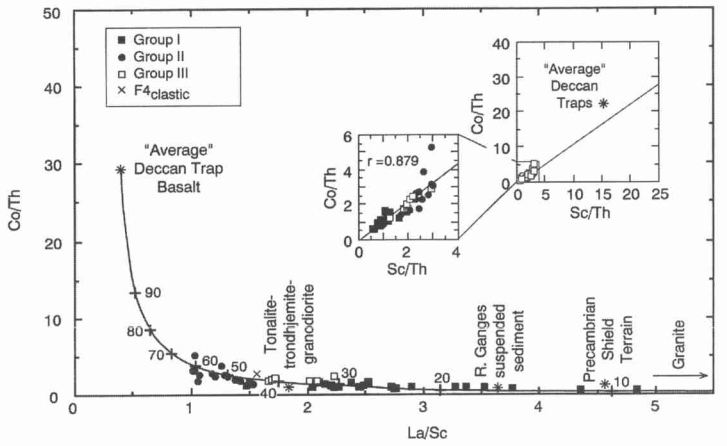

Fig. 13. Co/Th–La/Sc diagram showing the distribution of distal Bengal Fan sediments. An assessment of the possible proportionate contribution of sources to the different lithofacies groups has been made assuming basaltic and granitic end-members. Crosses (+) show mixing proportions in 10% increments. Basalt composition is an 'average' value calculated from Deccan Trap data reported in Lightfoot (1985). Phanerozoic granite is taken from Condie (1993). See Fig. 6 for all data sources except Phanerozoic tonalite–trondhjemite–granodiorite (TTG), for which data are taken from Condie (1993). Internal consistency of two-component mixing is supported by the linear correlation between Co/Th–Sc/Th (inset). The correlation coefficient is calculated using Bengal Fan data only.

Hansen *et al.* 1995) available as a source of sediment supply to the Bengal Fan (see also Einsele *et al.* 1996). Although estimates for the average geochemical composition of the Indian Shield are not currently available, the present-day 'Canadian Precambrian Shield estimate' of Shaw *et al.* (1986) represents a possible proxy for Precambrian terrains world-wide and displays a number of features consistent with those expected if sediments equivalent in composition to Group II turbidites were produced by mixing of detritus derived from erosion of basaltic (Deccan Traps) and tonalitic (Precambrian Indian Shield) crust of the Indian subcontinent (see Figs 13 and 14). Bimodal mixing of sediments similar in composition to the Canadian Precambrian Shield estimate and Deccan Trap basalts are clearly capable of meeting many of the criteria demanded by trace element data.

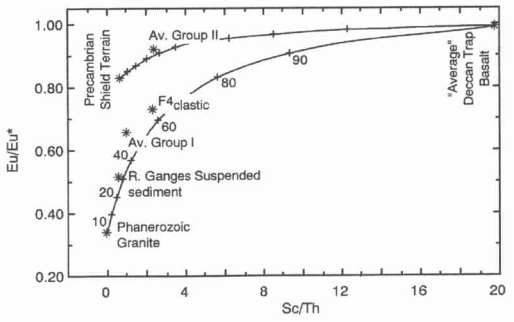

Fig. 14. Eu/Eu*–Sc/Th diagram illustrating the effects of bimodal mixing of sediment derived from tonalitic Precambrian Shield terrain and granite with Deccan Trap basalt. Crosses (+) show mixing proportions in 10% increments. Note that River Ganges suspended sediment and average Group I lithofacies plot close to the basalt–granite mixing line, while average Group II lithofacies plot close to the basalt–Precambrian shield terrain mixing line. Mean values for each lithofacies are used for clarity (distribution of all distal Bengal Fan data is shown in Fig. 8). See Fig. 6 for details of all data sources except Phanerozoic granite, for which data are taken from Condie (1993).

Group III. Estimates of the trace element geochemistry of the clastic component ($F4_{clastic}$) of Group III lithofacies reveal strong compositional affinities with Group II turbidites. Similarities in the behaviour of the transition metals (Co, Cr, Fe, Ti, Sc enrichment) and large ion lithophile elements (K, Rb, Th depletion) suggest that carbonate-rich sediments were derived from the same Indian subcontinent provenance invoked as the source of Group II deposits. However, the clastic component of Group III turbidites is relatively depleted in Eu (Eu/Eu* *c.* 0.72) compared to most Group II samples and consequently requires an increased contribution from an Eu-depleted, differentiated granitic crustal source to account for this.

Stow *et al.* (1990) have previously inferred a Sri Lankan origin for Group III turbidites in order to

account for the source of a bioclastic component (notably benthic foraminifera) of supposed shallow marine equatorial origin present in these sediments. A Sri Lankan source, dominated by late Archaean granulites (Newton & Hansen 1986), may be capable of accounting for the geochemistry of Group III turbidites. However, as with the Precambrian rocks of southern India, it is difficult to estimate the likely average geochemical composition of detritus eroded from Sri Lanka. A source terrain composition similar to the Precambrian Shield estimate of Shaw *et al.* (1986) fails to satisfy many of the geochemical characteristics displayed by the clastic component of Group III turbidites (depleted Eu/Eu*, low La/Sc, high Sc/Th and Cr/Th). The addition of a granitic crustal component with a depleted Eu anomaly may modify Eu/Eu* (Fig. 14), but would also require a contribution from mafic sources to account for the relatively high Co, Cr, Sc contents of these sediments. At present, insufficient data are available to allow us to evaluate fully a Sri Lakan/southern India provenance for Group III turbidites on a geochemical basis.

Nd and Sr isotopic data

Nd isotopic data. Although France-Lanord *et al.* (1993) state that the Nd isotopic data obtained from fan deposits are not consistent with an Indian Shield or Deccan Trap provenance, comparisons between published isotopic data from Precambrian rocks of southern India (e.g. Peucat *et al.* 1989;

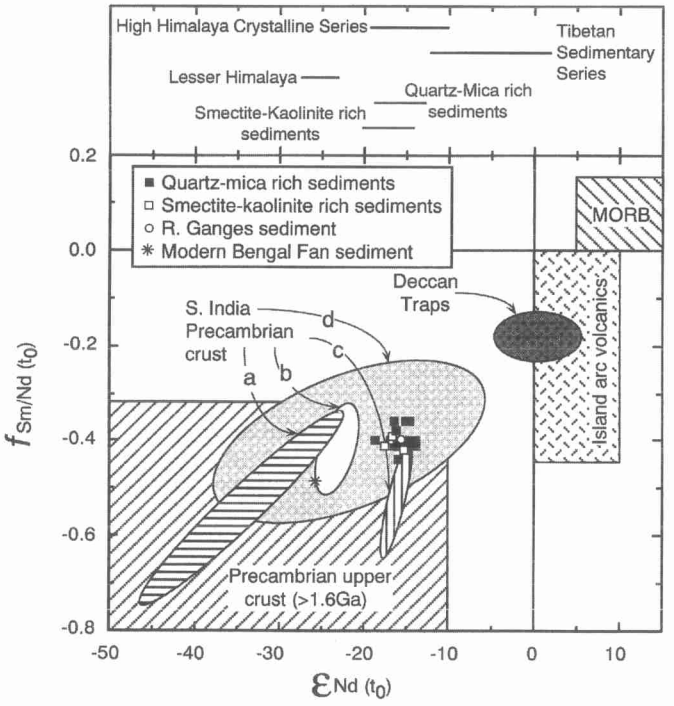

Fig. 15. Plot of f $Sm/Nd_{(t0)}$–$\varepsilon Nd_{(t0)}$ showing the Nd isotopic composition of distal fan sediments (quartz–mica and smectite–kaolinite turbidites of France Lanord *et al.* (1993) equate with Group I and Group II lithofacies respectively), River Ganges suspended sediment and Recent Bengal fan sediment relative to possible southern India Precambrian and Deccan Trap sources. The narrow range of $\varepsilon Nd_{(t0)}$ is consistent with the typical range of values observed in many Phanerozoic sediments (Goldstein 1988). The scatter of points suggests contributions from three or more isotopically distinct crustal sources (bimodal mixing should be characterized by a linear array). $\varepsilon Nd(t_0)$ and f Sm/Nd were calculated using present-day values of 0.512636 and 0.325 for $^{143}Nd/^{144}Nd_{CHUR}$ and Sm/Nd_{CHUR} respectively (DePaolo 1988; McLennan & Hemming 1992). Data sources: Distal Bengal Fan sediments, Lesser Himalaya, High Himalayan Crystalline Series, Tibetan Sedimentary Series (Bouquillon *et al.* 1990; France-Lanord *et al.* 1993); modern Bengal Fan sediment (McLennan *et al*, 1990); River Ganges sediment (Goldstein *et al.* 1984); S. India Precambrian crust: (a) Peucat *et al.* (1989); (b) Paul *et al.* (1990); (c) Burton & O'Nions (1990); (d) Harris *et al.* (1994); Deccan Traps (Lightfoot 1985); fields for Precambrian upper crust, island arc volcanics and MORB from McLennan & Hemming (1992).

Burton & O'Nions 1990; Paul *et al.* 1990; Harris *et al.* 1994), the Deccan Traps (Lightfoot 1985) and the Bengal Fan (Fig. 15) suggest that observed $^{143}Nd/^{144}Nd$ values could be explained if turbidite sediments were either derived directly from the Indian Shield or involved mixing of Precambrian crust with material eroded from the Deccan Traps. The potential importance of an Indian subcontinent source to distal fan sedimentation is further supported by a single isotopic value from Recent sediments recovered from the western margin of the Bengal Fan (McLennan *et al.* 1990) which gives an $\varepsilon Nd_{(t0)}$ (–25.7) consistent with a Precambrian Indian subcontinent source (see Fig. 15).

The similarity between the geochemical and isotopic composition (see Fig. 15) of modern River Ganges suspended sediment and quartz–mica Group I turbidites overwhelmingly supports the conclusion that these distal fan sediments were derived from erosion of the Himalayas. In contrast, interpretation of geochemical data obtained from smectite–kaolinite Group II and Group III turbidites indicates that these sediments were sourced by a mixture of detritus derived from the Precambrian Shield and the Deccan Trap basalts rather than granitic, upper crustal rocks exposed in the Himalayas. In order to test this hypothesis with respect to Nd isotopes we constructed a bimodal mixing model using published data from Precambrian Shield and Deccan Trap rocks.

Figure 16 illustrates the results of the model and demonstrates that mixing of Deccan Trap and Precambrian Shield-derived detritus could reasonably account for the range of isotopic values observed for smectite–kaolinite turbidites. Importantly, the mixing ratios calculated from Nd isotopic data are

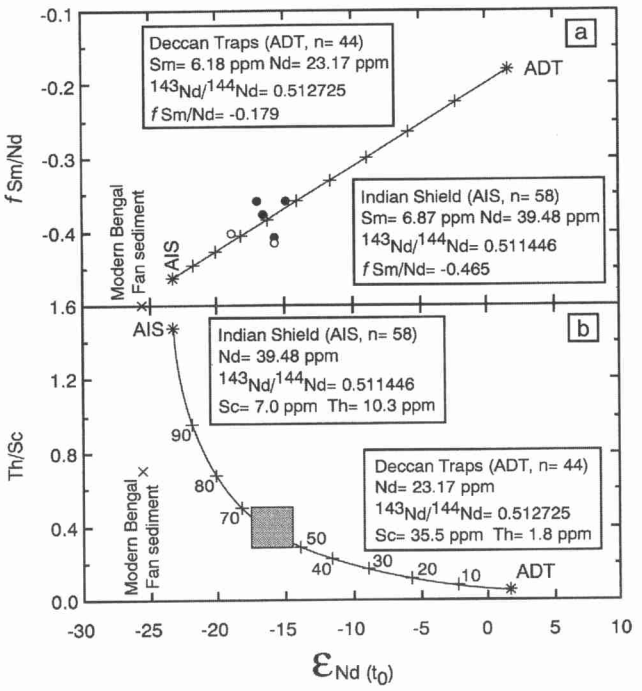

Fig. 16. (**a**) f $Sm/Nd_{(t0)}$–$\varepsilon Nd_{(t0)}$ and (**b**) Th/Sc–$\varepsilon Nd_{(t0)}$ mixing models for sediment derived from the Indian subcontinent. Data plotted in (a) are compositions of smectite–kaolinite turbidites (filled circles, F3; open circles, $F4_{gr}$) taken from Bouquillon *et al.* (1990) and France-Lanord *et al.* (1993). Shaded area in (b) shows the range of Th/Sc and $\varepsilon Nd_{(t0)}$ values for smectite–kaolinite (lithofacies F3) samples. The two-component mixing lines were calculated using an average value for Deccan Trap basalts calculated from the data of Lightfoot (1985; Mahabaleshwar, Panhala, Ambenali, Poladpur Formations) and an average value for the Indian shield calculated from the data of Peucat *et al.* (1989), Paul *et al.* (1990), Burton & O'Nions (1990) and Harris *et al.* (1994; not including samples 32D, 32F). Sc and Th composition of the Indian shield was assumed to be identical to the Canadian Precambrian Shield estimate of Shaw *et al.* (1986). Crosses (+) show mixing proportions in 10% increments. Recent Bengal Fan sediment data from McLennan *et al.* (1990). $\varepsilon Nd(t_0)$ and f Sm/Nd were calculated using present-day values defined in Fig. 15.

similar to those required to model successfully other features of the geochemistry of these Group II sediments (compare Figs. 13, 14, 16). For bimodal mixing a linear array of isotopic values would ideally be expected. In practice the small quantity of data (complete Sm, Nd and $^{143}Nd/^{144}Nd$ are only available for six samples) published for these turbidites define only a weak covariant trend and are insufficient in number to allow bimodal mixing to be evaluated fully. Furthermore, although two major source terrains (i.e. Deccan Traps and Indian Shield) are invoked to account for the geochemical composition of Group II turbidites, the diverse lithological make-up of the Indian Shield would indicate that a simple bimodal mixing model is unlikely to account precisely for the distribution of Nd isotopic data. Despite these uncertainties, it is sufficient to note that Nd isotope signatures preserved in distal fan sediments are not unique to a Himalyan source, and that mixing of detritus derived from the Indian Shield and the Deccan Traps can account for Nd isotopic data in samples where mineralogical and geochemical data are consistent with an Indian subcontinent provenance. Additional isotopic analyses of Group II and Group III lithofacies, together with modern sediment samples from Indian subcontinent rivers, are required to test this model further.

Sr isotopic data. As with Nd isotopic data, the Sr isotopic composition of distal fan sediments (particularly Group II turbidites) could be explained by mixing of young, Rb-depleted basaltic material (Lightfoot 1985) with radiogenic Precambrian crust (e.g. Taylor *et al.* 1984; Paul *et al.* 1990; Bhaskar Rao *et al.* 1992; Sarkar *et al.* 1993). The routine application of strontium isotopic data to provenance studies is, however, less reliable than $^{143}Nd/^{144}Nd$ because of the effects of differential chemical weathering on isotopic signatures preserved in clastic sediments (Goldstein 1988; Nelson & DePaolo 1988). Although Sr isotopes may provide a potentially unreliable indicator of sediment provenance, the data do allow us to test the 'variable weathering of a common source terrain' model proposed by France-Lanord *et al.* (1993) to account for differences in sediment mineralogy and similarities in $^{143}Nd/^{144}Nd$.

Because chemical weathering processes result in the progressive (and mineralogically selective) loss of Sr relative to Rb with increased weathering (Taylor & McLennan 1985), Rb/Sr ratios of sediments are frequently modified to give values greater than those present in source rocks (Nesbitt *et al.* 1980; Goldstein 1988; Nelson & DePaolo, 1988). The effect of Sr removal is reflected in the young Sr mantle-depleted model ages (T^{Sr}_{DM}) relative to Nd (T^{Nd}_{DM}) model ages calculated for the same sediment sample (Goldstein 1988; Nelson & DePaolo 1988). If the source of distal fan sediments remained constant, as suggested by France-Lanord *et al.* (1993), then it would be expected that T^{Sr}_{DM} ages should decrease systematically with progressive chemical weathering, while T^{Nd}_{DM} ages would remain constant due to the retention of Sm and Nd during weathering (Goldstein 1988; Nelson & DePaolo 1988; McLennan & Hemming 1992).

Although paired Sr and Nd data are only available for a small number of samples, it is clear that while Nd model ages fall within a narrow range, Sr model ages vary considerably (Fig. 17). Such behaviour is consistent with the effects of increased chemical weathering. However, the data show no systematic relationship between model age and smectite content (used as a measure of weathering intensity) which would indicate that the variation in sediment mineralogy was due to differences in the degree of weathering of a common crustal source (Fig. 17). In this respect Sr isotope values support the contention based on geochemical data that these sediments were derived from source terrains of differing bulk composition.

Changes in sediment provenance during fan deposition

Changes in sediment provenance with respect to time are conveniently represented by variations in the Cr/Th and Eu/Eu* (Fig. 18). The overall pattern of change in sediment provenance during the preceding *c.* 17.5 Ma is similar to that reported by Cochran (1990), Stow *et al.* (1990) and Amano & Taira (1992). Changes in sediment provenance with respect to time are summarized below (no geochemical data are available for recent deposits of <0.05 Ma):

0.05–0.73 Ma: quartz–mica turbidites derived from the Himalayan provenance;
0.73–3.40 Ma: smectite–kaolinite mud turbidites and bioclastic turbidites derived from the Indian subcontinent and Sri Lanka;
3.40–6.90 Ma: mixed provenance comprising turbidites sourced from the Indian subcontinent and the Himalayas.
6.90–17.5 Ma: quartz–mica turbidites derived from the Himalayas, with minor volumes of sediment sourced from the Indian subcontinent.

Although it is obvious that the bulk of sediment reaching the Bengal Fan has been sourced by erosion of the Himalayas (Curray & Moore 1971; Curray 1994; Johnson 1994; Einsele *et al.* 1996)

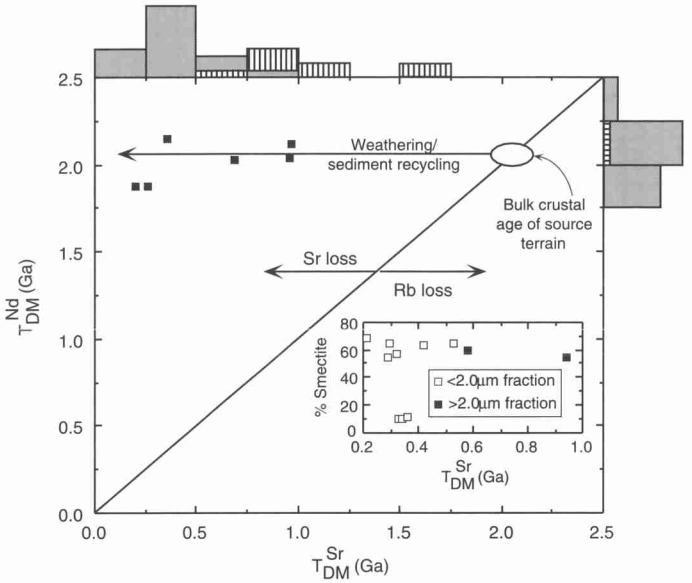

Fig. 17. Plot of T^{Sr}_{DM}–T^{Nd}_{DM} for Bengal fan sediments (all data from Bouquillon *et al.* 1990; France-Lanord *et al.* 1993). Samples were decarbonated with 10% acetic acid. Note that Sr mantle-depleted model ages are considerably younger than equivalent Nd ages consistent with Sr loss and Nd retention during weathering and transport of clastic detritus. Histograms show the mantle-depleted age distribution of all available (unpaired) isotopic data. Sr model ages show a wide spread of values with clay fraction samples (<2 μm; stippled infill) giving younger ages than coarser fraction samples (>2 μm; lined infill). Inset diagram shows the relationship between Sr model age and smectite content of individual fan samples. The data reveal no systematic relationships which would be consistent with progressive weathering of a common crustal source. Model ages were calculated using the depleted mantle parameters of Goldstein & Jacobsen (1988), and McLennan & Hemming (1992) for Sr and Nd respectively.

and transported *via* the Ganges–Brahamaputra dispersal system, it is not at all certain why the record of deposition on the distal fan should be interrupted by significant periods (up to 2.5 Ma) of turbidite sedimentation involving material derived predominantly from the Indian subcontinent. Assuming a continuous, high rate of terrigenous sediment transport to the Bay of Bengal (Copeland & Harrison (1990), although see Rea (1992) for a broader perspective of the relationship between Himalayan uplift and sediment supply to the northern Indian Ocean), it might be expected that sediment supply to the distal fan would be controlled predominantly by changes in relative sea level (Stow *et al.* 1983, 1990). Under these circumstances sediment supply to the Bengal Fan may be divided into: (1) periods of thick, relatively coarse-grained, quartz–mica turbidite sedimentation corresponding to low-stands associated with fluvial incision and efficient sediment bypassing of the Bengal shelf; and (2) periods of clay-rich, smectite–kaolinite turbidite deposition corresponding to high-stands when shorelines migrate landwards allowing Himalayan-derived sediment to be stored on the Bengal shelf, while Indian subcontinent-derived sediment continued to be transported across the much narrower Indian continental margin.

Comparisons between the distal fan sedimentary record and eustatic sea level (Stow *et al.* 1990; Fig. 18) show that low-stand periods correlate only in a general sense with the occurrence of thick, coarser-grained Himalayan-derived turbidite sequences. Of particular importance is the relative absence of quartz–mica turbidites at the site of Leg 116 during the Pliocene and early Pleistocene when two periods of major sea-level fall occur. Evidence from modern Bengal shelf sediment dispersal patterns (Kuehl *et al.* 1989) suggests that efficient sediment bypassing of the shelf occurs even at relatively high, present-day sea levels. As a consequence Himalayan-derived sediment should continue to reach distal portions of the fan, even during relative high-stands, and this is supported by the deposition of Himalayan-derived turbidites on the distal fan during 3.4–6.9 Ma when estimated

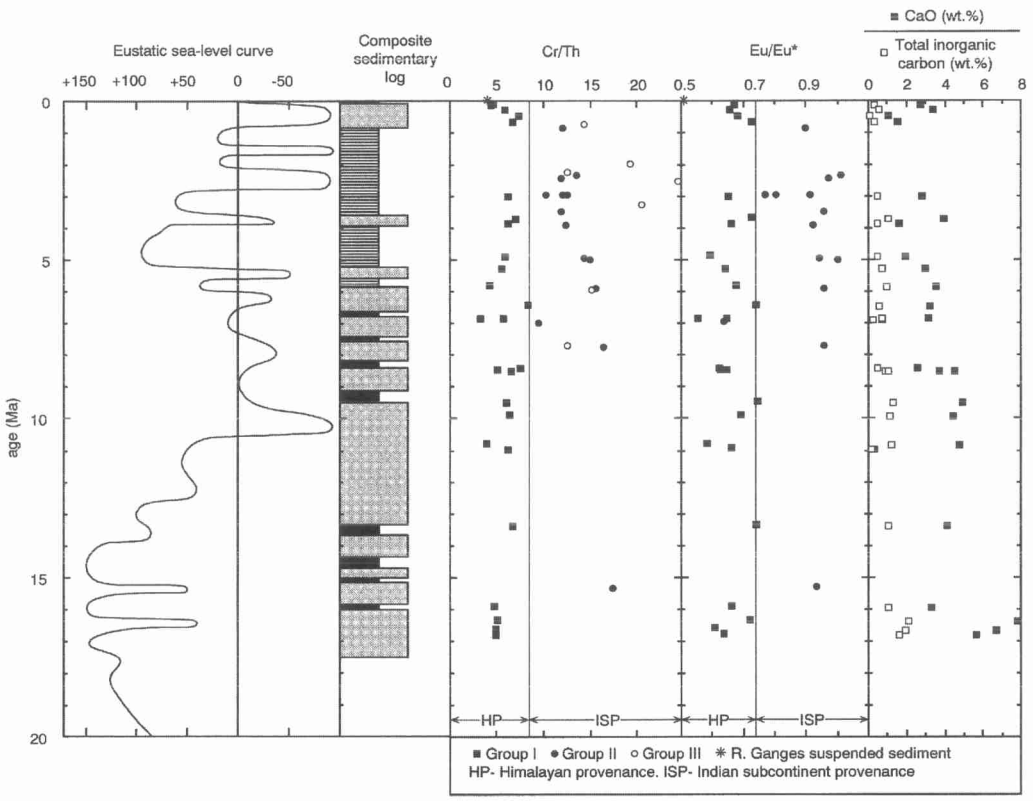

Fig. 18. Variation in sediment provenance with respect to time using Cr/Th (all data) and Eu/Eu* (from Group I and Group II turbidites only). Composite log of distal fan sedimentation and eustatic sea-level curve from Stow *et al.* (1990; symbols as for Fig. 2). River Ganges suspended sediment data from Martin & Maybeck (1979). CaO and TIC data from Group I turbidites only. The general increase in CaO and TIC with time suggests that the abundance of carbonate-containing source rocks (notably limestones and marbles present in the Tibetan Sedimentary Series and High Himalaya Crystalline Series) has decreased progressively since the Lower Miocene.

eustatic sea levels were over 50 m higher than the present-day.

Stow *et al.* (1990) have previously noted that changes in the position of major distributary fan channels, leading to a shift in sediment supply either to the currently abandoned easterly fan lobe of the Bengal Fan or the Nicobar Fan, could account for the occurrence of prolonged periods when little or no sediment derived from the Himalayan provenance reached distal fan sites of Leg 116. Assuming that Himalayan detritus was continuously reaching the Bay of Bengal submarine canyon, it would appear highly unlikely that relatively small-scale, medial to distal fan autocyclic sedimentary processes could account for significant periods of non-deposition and that regional-scale changes such as channel avulsion and lobe switching are required. If periodic fan-lobe abandonment did occur for significant lengths of time then sediment supply to the distal fan would be relatively insensitive to sea-level change affecting the northern Bay of Bengal and would allow turbidites transported from the Indian subcontinental margin to accumulate in the absence of sediment derived from the Himalayas. Under these circumstances attempts to reconstruct major Himalayan tectonic and climatic events based on data obtained from the sedimentary record of the distal Bengal Fan may prove to be unreliable.

Conclusions

(1) Whole-rock mineralogical and geochemical investigation of samples recovered during ODP Leg 116 allow sediments to be resolved into three distinct groups consistent with major depositional lithofacies associations recognized in distal Bengal Fan cores.

(2) Estimates of the intensity of source-area chemical weathering based on CIA are consistent with the clay mineralogy of distal fan sediments. A–C*N*–K and Th/U–Th diagrams reveal important differences in the pattern of behaviour of quartz–mica and smectite–kaolinite turbidites with respect to changes in chemical weathering intensity. The most likely explanation for these differences is that they result from variations in the degree of chemical weathering of two different source terrains as opposed to differential weathering of a single source terrain of relatively uniform composition.

(3) Turbidites characterized by high concentrations of quartz and mica (Group I lithofacies) have trace element compositions consistent with erosion of a source terrain similar in bulk composition to Upper Continental Crust. Both mineralogical and geochemical signatures are compatible with a Himalayan source consisting of (meta) clastic sediments, granites and minor quantities of basalt.

(4) Organic-rich turbidites (Group II lithofacies), characterized by high concentrations of smectite and kaolinite, have trace element compositions which indicate a source containing a mixture of basaltic and tonalitic crust. Such a source is consistent with erosion of Deccan Trap basalts and Precambrian Shield terrains of the Indian subcontinent.

(5) The clastic component of carbonate-rich turbidites (Group III) exhibits many of the mineralogical and trace element characteristics displayed by Group II turbidites and indicates that a similar Indian subcontinent provenance is probable for these sediments. Although a Sri Lankan source has been proposed for these sediments on the basis of faunal content, geochemical data alone are insufficient to allow a Sri Lankan source to be reliably identified.

(6) Nd isotopic signatures published for smectite–kaolinite (Group II and Group III lithofacies) turbidites are not unique to a Himalayan source. Modelling of Nd isotopes shows that similar $\varepsilon Nd_{(t0)}$ values to those reported from the High Himalaya and distal fan sediments can be obtained by mixing of detritus derived from the Precambrian Shield and Deccan Trap basalts of the Indian subcontinent. Importantly, the mixing ratios obtained on the basis of Nd isotopic data are similar to those required to model successfully other features of the geochemistry of these sediments, and this further supports an Indian subcontinent provenance for these turbidites.

(7) Changes in the provenance of turbidites over the last *c.* 17.5 Ma indicate significant variation in the supply of Himalayan-derived sediment to the distal fan. The most likely causes of observed patterns of sediment supply are thought to be related to an interplay between sea-level change and distributary channel switching. As a consequence, attempts to reconstruct major Himalayan tectonic and climatic events based on data obtained from the sedimentary record of the distal Bengal Fan may be unreliable.

Appendix

Analytical results of 46 samples from Sites 717 and 718

Sample No. (ODP core ref)	Depth (mbsf)	Age (Ma)	Facies	SiO_2 (%)	Al_2O_3 (%)	TiO_2 (%)	Fe_2O_3T (%)	MgO (%)	CaO (%)	Na_2O (%)	K_2O (%)	MnO (%)	P_2O_5 (%)	LOI (%)	Total (%)	$Na_2O^{\dagger}$ (%)	Na_2O^{*} (%)	TOC (%)	TIC (%)
Hole 717C																			
2.2.35–40	15.35	0.16	1	70.60	11.24	0.54	4.20	2.09	2.73	2.13	2.63	0.06	0.10	3.83	100.15	0.42	1.71	0.15	0.32
6.1.53–55	46.53	0.29	2	57.48	15.99	0.76	5.92	3.30	3.40	2.25	3.79	0.09	0.14	6.91	100.03	0.47	1.78	0.46	0.55
10.1.110–112	75.61	0.47	2	54.08	18.37	0.86	8.60	3.15	1.08	2.17	3.63	0.09	0.13	7.89	100.05	0.96	1.21	0.66	0.05
18.CC.8–12	131.58	0.67	1	78.17	9.83	0.24	2.98	0.90	1.55	2.11	2.49	0.05	0.06	1.68	100.06	0.25	1.86	0.57	0.35
20.4.36–41	155.36	0.76	4gr	35.03	12.28	0.71	6.56	2.54	17.03	1.47	1.57	0.11	0.22	22.44	99.96	0.85	0.62	1.88	3.77
23.5.140–145	186.41	0.87	3	50.72	17.25	1.20	10.41	3.03	2.10	1.36	2.47	0.12	0.13	10.95	100.31	0.69	0.40	1.56	0.47
27.5.85–89	223.85	2.01	4gr	25.98	9.02	0.46	5.67	2.04	24.23	1.13	0.64	0.24	0.26	30.36	100.03	0.84	0.29	5.64	2.51
28.5.102–106	233.52	2.29	4gr	13.98	4.00	0.19	2.72	1.38	39.88	0.51	0.07	0.93	0.64	35.37	99.67	0.84	0.03	0.66	8.21
29.2.80–86	238.31	2.34	3	50.75	16.33	1.69	11.01	2.66	1.97	2.34	2.01	0.12	0.13	11.12	100.13	1.09	1.25	1.93	0.38
30.1.111–116	246.61	2.44	7dg	45.55	16.08	1.37	16.40	2.46	0.74	2.02	1.79	0.12	0.11	13.50	100.14	0.77	1.25	1.87	0.29
31.1.55–57	255.55	2.57	4gr	20.24	7.71	0.38	5.65	1.94	29.59	1.05	0.33	0.42	0.93	31.06	99.30	1.03	0.02	1.27	6.79
33.5.80–85	280.80	2.94	3	48.65	18.25	1.25	10.06	2.64	2.37	1.96	2.27	0.14	0.10	12.35	100.04	0.78	1.18	2.30	0.38
33.5.120–122	281.20	2.95	3	51.01	18.50	1.33	9.71	2.62	1.86	1.98	2.60	0.12	0.12	10.40	100.25	nd	nd	1.37	0.17
33.6.31–33	281.81	2.96	3	52.47	17.64	1.26	12.27	2.79	0.47	2.12	2.01	0.06	0.09	8.84	100.01	nd	nd	0.60	bdl
34.1.53–55	284.03	3.00	2	53.77	17.21	0.84	7.59	3.28	2.85	1.93	3.93	0.13	0.10	8.29	99.92	0.75	1.18	0.38	0.49
35.3.46–51	296.46	3.25	4gr	33.85	13.43	0.68	10.36	2.80	13.33	1.25	1.25	0.21	0.41	22.52	100.09	0.82	0.43	3.36	2.15
36.5.80–85	309.31	3.46	3	46.59	20.28	1.52	10.68	2.37	1.70	1.73	1.98	0.13	0.12	12.89	99.99	0.89	0.84	2.06	0.50
39.1.82–87	331.82	3.69	1	58.31	14.33	0.88	6.47	2.70	3.98	2.07	3.13	0.09	0.12	7.99	100.07	0.59	1.48	0.72	1.05
40.1.103–108	341.53	3.85	2	56.07	17.06	0.79	8.23	2.94	1.59	1.90	3.70	0.21	0.11	7.41	100.01	0.63	1.28	0.52	0.46
40.3.117–123	344.67	3.91	3	43.33	16.30	1.00	9.27	2.25	8.23	1.76	1.96	0.06	0.24	15.32	99.72	1.07	0.69	0.48	2.73
47.3.80–85	410.81	4.87	7lg	54.98	17.68	0.78	7.84	2.87	1.93	1.77	3.79	0.13	0.11	8.15	100.03	0.57	1.20	0.64	0.49
47.CC.33–38	416.11	4.94	7dg	48.91	18.91	1.61	10.82	2.24	1.78	1.84	1.81	0.09	0.10	11.90	100.01	0.82	1.02	2.18	0.30
48.2.80–86	418.81	4.98	3	50.86	17.75	1.47	12.59	2.46	0.55	2.00	1.93	0.05	0.11	10.40	100.17	0.77	1.24	1.61	bdl
50.1.11–16	435.61	5.27	2	56.59	16.22	0.76	6.76	2.90	2.99	1.89	3.97	0.15	0.11	7.63	99.97	0.61	1.28	0.43	0.75
53.1.104–108	465.04	5.81	1	70.06	10.37	0.54	4.04	1.97	3.56	1.82	2.54	0.07	0.10	5.30	100.37	0.42	1.40	0.17	0.95
54.5.126–131	480.76	5.90	3	49.12	19.26	1.50	11.03	2.44	0.74	1.97	1.56	0.07	0.09	12.46	100.24	0.63	1.34	2.32	0.20
55.CC.23–28	482.83	5.93	4gr	44.19	15.41	0.84	9.41	2.57	9.46	1.62	1.98	0.18	0.18	14.40	100.24	0.85	0.77	0.62	1.93
59.3.121–126	525.21	6.43	7lg	54.73	16.95	0.85	7.28	2.84	3.23	1.77	3.53	0.20	0.11	8.39	99.88	0.64	1.13	0.54	0.57
62.CC.11–15	559.46	6.84	1	74.75	8.99	0.53	3.14	1.45	3.19	1.75	2.09	0.06	0.09	4.09	100.14	0.31	1.44	0.10	0.70
63.2.42–47	560.92	6.86	2	53.34	18.54	0.83	10.39	3.19	0.71	1.29	4.53	0.10	0.10	6.72	99.73	0.42	0.87	0.30	0.24
64.1.53–55	569.03	6.96	7dg	48.37	15.81	0.94	10.02	2.58	6.76	1.49	2.56	0.09	0.11	11.36	100.09	0.78	0.71	0.40	1.10
70.5.63–69	632.13	7.71	4gr	41.95	12.99	0.93	8.82	2.35	13.73	1.46	1.45	0.09	0.11	16.32	100.20	0.85	0.61	1.03	0.65
70.5.95–100	632.45	7.72	3	46.73	17.12	1.57	13.84	2.28	2.69	1.87	1.39	0.13	0.09	12.49	100.20	0.82	1.05	1.30	0.58
79.6.91–96	719.41	8.41	2	54.90	17.87	0.79	7.12	3.12	2.57	1.73	3.56	0.18	0.13	8.16	100.13	0.54	1.19	0.69	0.50
81.CC.18–23	731.03	8.46	1	66.24	11.42	0.58	4.27	2.13	4.54	1.80	2.66	0.07	0.12	6.20	100.03	0.27	1.54	0.22	0.92
82.1.48–50	739.98	8.50	2	56.22	16.14	0.17	6.85	3.04	3.69	1.45	3.70	0.11	0.11	7.85	99.87	0.46	1.01	0.41	1.02
Hole 718C																			
46.1.53–55	437.33	9.49	2	55.57	15.14	0.71	5.74	3.33	4.90	1.57	3.42	0.13	0.11	8.96	99.59	0.56	1.01	0.23	1.33
50.1.60–63	475.41	9.89	2	53.07	16.84	0.75	6.65	3.52	4.41	1.55	3.75	0.11	0.14	9.03	99.82	0.62	0.93	0.24	1.13
59.2.87–92	562.67	10.80	1	71.91	8.93	0.51	2.72	1.76	4.79	1.72	1.94	0.04	0.12	5.66	100.11	0.36	1.36	0.01	1.18
65.2.53–55	619.33	10.96	1	62.08	16.71	0.76	7.04	2.52	0.31	1.49	3.91	0.05	0.11	4.79	99.78	0.46	1.03	0.01	0.16
72.2.46–51	685.76	13.38	1	62.43	12.95	0.62	5.21	2.82	4.13	1.40	2.95	0.08	0.11	7.27	100.03	0.38	1.07	0.21	1.06
79.1.53–55	750.83	15.35	5r	50.99	22.44	1.02	10.57	2.91	2.19	1.84	2.49	0.11	0.12	11.68	100.19	0.59	1.25	0.11	0.27
81.1.52–54	769.82	15.93	2	53.82	17.69	0.73	6.89	3.03	3.29	1.13	4.42	0.13	0.13	8.73	99.99	0.41	0.72	0.40	1.06
87.1.53–55	826.83	16.36	2	49.73	15.19	0.62	5.71	3.66	7.81	0.94	4.01	0.09	0.11	12.33	100.21	0.39	0.55	0.39	2.10
96.1.20–22	905.71	16.64	2	52.91	14.66	0.67	5.39	3.53	6.73	1.12	3.82	0.09	[illegible]	10.93	100.06	0.39	0.73	0.30	1.94
3R.2.15–17	953.75	16.80	2	51.37	16.31	0.67	5.92	3.72	5.64	1.11	4.41	0.09	[illegible]	10.61	99.98	0.42	0.69	0.46	1.59

Sample No. (ODP core ref)	S (%)	CIA	Co (ppm)	Cr (ppm)	Cs (ppm)	[illegible] (ppm)	Rb (ppm)	Sc (ppm)	Ta (ppm)	Th (ppm)	U (ppm)	La (ppm)	Ce (ppm)	[illegible] (ppm)	Sm (ppm)	Eu (ppm)	Tb (ppm)	Tm (ppm)	Yb (ppm)	Lu (ppm)
Hole 717C																				
2.2.35–40	0.01	57.4	11.8	56.0	7.2	5.6	162	9.23	1.18	12.49	2.29	32.5	65.8	26	5.12	1.00	0.62	0.36	2.12	0.37
6.1.53–55	0.03	63.1	21.4	110.0	13.0	4.4	207	16.76	1.68	18.75	2.96	41.6	90.7	36	6.90	1.38	0.97	0.36	2.65	0.46
10.1.110–112	0.01	69.0	28.0	139.0	14.0	3.8	195	22.43	1.62	18.86	2.70	45.7	97.6	37	7.68	1.57	1.02	0.36	2.82	0.43
18.CC.8–12	bdl	61.3	6.5	57.0	3.1	3.5	110	6.29	0.76	8.38	1.46	23.7	46.6	15	3.11	0.69	0.44	0.21	1.44	0.28
20.4.36–41	0.72	nd	17.2	117.0	4.1	2.7	95	16.43	0.76	8.42	5.42	27.8	56.0	24	5.37	1.06	0.65	0.29	1.96	0.34
23.5.140–145	0.22	81.8	29.3	153.0	5.9	3.5	134	29.29	1.28	12.54	2.15	38.4	84.5	26	5.10	1.55	0.98	0.34	2.40	0.40
27.5.85–89	2.22	nd	11.7	127.0	2.6	2.0	69	12.35	0.52	6.70	7.83	25.6	50.6	22	4.97	0.88	0.58	0.30	2.05	0.29
28.5.102–106	bdl	nd	7.9	40.0	1.8	0.9	29	6.95	0.27	3.20	2.12	15.5	28.0	13	2.88	0.74	0.49	0.25	1.70	0.24
29.2.80–86	1.15	76.3	32.7	163.0	3.8	4.3	97	29.00	1.17	11.99	2.49	34.2	72.1	22	4.70	1.62	0.93	0.35	2.12	0.38
30.1.111–116	5.22	80.1	40.4	125.0	3.3	3.3	79	27.65	0.98	10.43	2.28	34.8	65.6	21	4.57	1.50	0.87	0.31	2.13	0.31
31.1.55–57	2.12	nd	8.6	114.0	1.3	1.0	42	9.15	0.32	4.65	5.55	18.4	34.0	14	3.29	0.64	0.42	0.19	1.31	0.21
33.5.80–85	0.50	75.1	34.6	158.0	6.9	3.5	124	29.80	1.24	13.06	2.78	38.2	79.9	24	5.39	1.66	1.03	0.34	2.57	0.45
33.5.120–122	0.43	nd	27.9	149.0	6.8	3.6	124	27.94	1.29	14.49	2.85	38.5	79.1	35	7.79	1.86	1.01	0.50	3.10	0.50
33.6.31–33	0.16	nd	22.0	160.0	4.7	3.3	111	30.69	1.10	12.60	1.40	32.7	69.7	31	7.25	1.67	0.97	0.48	2.85	0.42
34.1.53–55	0.01	69.2	18.5	111.0	15.2	3.9	191	20.70	1.45	17.85	2.06	42.3	85.1	34	7.57	1.50	1.06	0.37	2.93	0.51
35.3.46–51	1.55	nd	19.1	177.0	3.1	2.3	81	17.04	0.58	8.34	3.42	29.2	58.9	20	5.00	1.11	0.65	0.29	2.17	0.34
36.5.80–85	0.32	85.2	31.2	163.0	5.4	4.1	101	34.80	1.22	13.54	2.01	42.0	78.3	27	5.70	1.80	1.02	0.34	2.70	0.46
39.1.82–87	0.23	70.2	21.9	97.0	10.9	5.7	159	16.93	1.49	13.80	2.41	35.3	78.5	33	6.32	1.40	0.89	0.40	2.56	0.45
40.1.103–108	0.12	73.6	21.1	115.0	13.8	4.5	197	19.15	1.44	18.60	2.62	42.0	87.5	34	7.37	1.44	0.95	0.35	2.83	0.52
40.3.117–123	0.74	83.4	19.8	154.0	5.7	2.9	109	24.00	1.05	12.29	3.06	35.9	69.8	20	4.68	1.43	0.84	0.29	2.25	0.38
47.3.80–85	0.31	74.0	18.5	110.0	14.5	3.8	238	18.67	1.50	18.87	2.93	42.3	87.2	29	7.82	1.35	0.95	0.50	3.35	0.48
47.CC.33–38	0.70	80.0	30.8	171.0	4.7	4.1	95	33.64	1.27	11.89	2.14	36.1	72.3	20	5.50	1.70	0.95	0.35	2.56	0.43
48.2.80–86	0.53	78.5	40.7	193.0	4.8	4.3	110	37.15	1.22	12.73	2.41	37.6	80.9	26	5.77	1.92	1.05	0.35	2.29	0.37
50.1.11–16	0.11	70.5	15.2	104.0	14.3	4.4	185	17.67	1.50	18.81	2.52	43.1	89.9	35	7.84	1.45	0.92	0.36	3.20	0.56
53.1.104–108	bdl	66.5	12.9	56.0	8.9	6.4	139	10.30	1.34	13.12	2.28	34.7	76.5	30	5.63	1.19	0.85	0.34	2.30	0.44
54.5.126–131	0.36	83.2	36.4	183.0	4.6	3.8	89	35.24	1.14	11.67	2.56	36.5	74.3	27	5.64	1.78	1.00	0.33	2.10	0.36
55.CC.23–28	0.53	nd	17.9	156.0	4.6	2.6	103	20.67	0.78	10.29	1.81	34.4	66.8	24	7.12	1.51	0.90	0.38	2.50	0.43
59.3.121–126	0.08	68.9	12.5	82.0	6.5	2.1	106	16.07	0.78	9.87	1.24	23.8	48.7	19	4.30	1.00	0.66	0.32	2.01	0.26
62.CC.11–15	bdl	61.0	8.9	48.0	5.8	9.0	118	8.62	1.31	14.79	2.52	41.7	90.8	35	7.61	1.23	0.95	0.35	2.70	0.51
63.2.42–47	0.86	74.5	19.8	113.0	15.7	5.0	250	20.20	1.52	19.75	2.28	45.3	91.8	36	7.70	1.49	1.03	0.36	2.92	0.52
64.1.53–55	bdl	nd	17.3	119.0	9.0	3.4	178	21.60	1.07	12.60	2.66	33.0	66.5	27	6.99	1.40	1.07	0.43	2.66	0.43
70.5.63–69	bdl	nd	21.8	113.0	4.6	3.2	82	22.58	0.86	9.17	1.60	33.2	63.1	26	7.38	1.79	1.19	0.45	3.10	0.47
70.5.95–100	2.04	80.3	58.9	185.0	4.5	4.1	89	32.83	1.19	11.16	2.77	34.0	69.6	24	5.03	1.64	0.98	0.36	2.50	0.41
79.6.91–96	0.16	71.9	22.7	131.0	13.8	4.5	177	19.82	1.36	17.44	2.70	42.5	85.7	33	8.05	1.41	0.89	0.34	2.73	0.51
81.CC.18–23	0.01	60.3	12.7	69.0	8.2	6.9	136	11.57	1.28	13.61	2.54	37.9	82.2	33	6.04	1.21	0.88	0.35	2.53	0.44
82.1.48–50	bdl	74.0	17.2	110.0	13.5	4.2	203	16.80	1.43	16.98	2.73	37.8	76.1	26	7.03	1.28	0.85	0.39	2.80	0.44
Hole 718C																				
46.1.53–55	bdl	73.2	16.5	103.0	11.1	4.2	192	15.89	1.43	16.85	2.80	39.0	80.9	33	5.62	1.30	0.84	0.35	2.59	0.40
50.1.60–63	bdl	73.5	18.5	115.0	12.9	4.1	209	17.57	1.48	17.94	2.89	39.2	83.3	34	6.39	1.32	0.84	0.38	2.60	0.51
59.2.87–92	bdl	63.0	7.0	48.0	4.6	6.3	101	7.39	1.03	12.05	2.26	32.2	65.4	27	5.55	0.96	0.71	0.36	2.18	0.40
65.2.53–55	bdl	73.8	26.4	102.0	12.6	4.4	237	17.37	1.44	16.50	2.28	41.1	85.3	35	7.19	1.39	0.89	0.39	2.74	0.55
72.2.46–51	bdl	70.4	20.0	81.0	9.2	4.2	165	12.71	1.23	12.16	2.18	32.0	66.1	27	4.87	1.10	0.69	0.39	2.25	0.40
79.1.53–55	bdl	76.9	21.4	218.0	5.4	3.2	86	25.91	1.05	12.48	2.05	36.8	80.1	25	4.87	1.49	0.85	0.31	2.02	0.35
81.1.52–54	bdl	74.8	16.0	97.0	12.2	4.2	231	16.73	1.51	20.14	3.04	46.0	95.1	40	7.77	1.45	0.87	0.42	2.86	0.53
87.1.53–55	bdl	72.3	14.9	83.0	9.6	3.8	208	14.71	1.24	16.11	2.63	40.0	83.6	33	5.86	1.25	0.76	0.40	2.41	0.46
96.1.20–22	bdl	73.3	14.2	78.0	8.4	4.1	188	13.54	1.29	17.75	2.99	39.2	80.7	32	6.76	1.21	0.86	0.40	2.49	0.49
3R.2.15–17	bdl	73.4	13.3	85.0	9.8	3.5	209	14.70	1.22	17.06	2.73	40.5	83.2	32	6.87	1.25	0.80	0.40	2.49	0.50

† Water-soluble fraction
* Silicate fraction

nd – not determined
bdl – below detection limits

References

AMANO, K. & TAIRA, A. 1992. Two-phase uplift of Higher Himalayas since 17Ma. *Geology*, **20**, 391–394.

AOKI, S., KOHYAMA, N. & ISHIZUKA, T. 1991. Sedimentary history and chemical characteristics of clay minerals in cores from the distal part of the Bengal fan. *Marine Geology*, **99**, 175–185.

ARGAST, S. & DONNELLY, T. W. 1987. The chemical discrimination of clastic sedimentary components. *Journal of Sedimentary Petrology*, **57**, 813–823.

BALSON, P. S. & STOW, D. A. V. 1990. Grain-size analysis: Leg 116, Bengal Fan. *In*: COCHRAN, J. R. & STOW, D. A. V. (eds) *Proceedings of the Ocean Drilling Program Leg 116, Scientific Results*. College Station, Texas, Ocean Drilling Program, 417–420.

BHASKAR RAO, Y. J., SIVARAMAN, T. V., PANTULU, G. V. C., GOPLAN, K. & NAQVI, S. M. 1992. Rb–Sr ages of late Archean metavolcanics and granites, Dhawar craton, south India and evidence for early Proterozoic thermotectonic event(s). *Precambrian Research*, **59**, 145–170.

BOUQUILLON, A., CHAMLEY, H. & FROHLICH, F. 1989. Sedimentation argileuse au Cenozoique superieur dans l'Ocean Indien nord-oriental. *Oceanologica Acta*, **12**, 133–147.

——, FRANCE-LANORD, C., MICHARD, A. & TIERCELIN, J.J. 1990. Sedimentology and isotopic chemistry of the Bengal fan sediments: the denudation of the Himalaya. *In*: COCHRAN, J. R. & STOW, D. A. V. (eds) *Proceedings of the Ocean Drilling Program Leg 116, Scientific Results*. College Station, Texas, Ocean Drilling Program, 43–58.

BRASS, G. W. & RAMAN, C. V. 1990. Clay mineralogy of sediments from the Bengal fan. *In*: COCHRAN, J. R. & STOW, D. A. V. (eds) *Proceedings of the Ocean Drilling Program Leg 116, Scientific Results*. College Station, Texas, Ocean Drilling Program, 35-41.

BRIQUEU, L., BOUGAULT, H. & JORON, J. L. 1984. Quantification of Nb, Ta, Ti and V anomalies in magmas associated with subduction zones: petrogenetic implications. *Earth and Planetary Science Letters*, **68**, 297–308.

BURTON, K. W. & O'NIONS, R. K. 1990. The timescale and mechanism of granulite formation at Kurunegala, Sri Lanka. *Contribributions to Mineralogy and Petrology*, **106**, 66–89.

COCHRAN, J. R. 1990. Himalayan uplift, sea-level, and the record of Bengal fan sedimentation at the ODP Leg 116 sites. *In*: COCHRAN, J. R. & STOW, D. A. V. (eds) *Proceedings of the Ocean Drilling Program Leg 116, Scientific Results*. College Station, Texas, Ocean Drilling Program, 397–414.

——, STOW, D. A. V. *ET AL.* 1989. *Proceedings of the Ocean Drilling Program Leg 116, Initial Reports*. College Station, Texas, Ocean Drilling Program.

——, ——, *ET AL.* 1990. *Proceedings of the Ocean Drilling Program Leg 116, Scientific Results*. College Station, Texas, Ocean Drilling Program.

CONDIE, K. C. 1991. Another look at rare earth elements in shales. *Geochimica et Cosmochimica Acta*, **55**, 2527–2531.

—— 1993. Chemical composition and evolution of the upper continental crust: contrasting results from surface samples and shales. *Chemical Geology*, **104**, 1–37.

—— & WRONKIEWICZ, D. J. 1990. The Cr/Th ratio in Precambrian pelites from the Kaapvaal Craton as an index of craton evolution. *Earth and Planetary Science Letters*, **97**, 256–267.

COPELAND, P. & HARRISON, T. M. 1990. Episodic rapid uplift in the Himalaya revealed by $^{40}Ar/^{39}Ar$ analysis of detrital K-feldspar and muscovite, Bengal fan. *Geology*, **18**, 354–357.

COX, K. G. 1989. The role of mantle plumes in the development of continental drainage patterns. *Nature*, **342**, 873–877.

CULLERS, R. L. 1994. The controls on the major and trace element variation of shales, siltstones, and sandstones of Pennsylvanian-Permian age from uplifted continental blocks in Colorado to platforr sediment in Kansas, USA. *Geochimica ϵ. Cosmochimica Acta*, **58**, 4955–4972.

CURRAY, J. R. 1994. Sediment volume and mass beneath the Bay of Bengal. *Earth and Planetary Science Letters*, **125**, 371–383.

—— & MOORE, D. G. 1971. Growth of the Bengal deep-sea fan and denudation in the Himalayas. *Geological Society of America Bulletin*, **82**, 563–572.

CURTIS, C. D. 1990. Aspects of climatic influence on the clay mineralogy and geochemistry of soils, palaeosols and clastic sedimentary rocks. *Journal of the Geological Society, London*, **147**, 351–357.

DEPAOLO, D. J. 1988. Age dependence of the composition of continental crust: evidence from Nd isotopic variations in granitic rocks. *Earth and Planetary Science Letters*, **90**, 263–271.

DERRY, L. & FRANCE-LANORD, C. 1991. Chemical and physical erosion in the Himalaya: an isotopic and mineralogical view from the Bengal Fan. *Eos* (Transactions of the American Geophysical Union), **72**, 257.

——, GALY, A. & FRANCE-LANORD, C. 1993. Himalayan erosion versus sedimentation in Bengal Fan. Evidence from geochemical and stratigraphic stud· of ODP Leg 116. *Terra Nova*, **5** (abstra supplement 1), 161.

EINSELE, G. RATSCHBACHER, L. & WETZEL, A. 1996. The Himalayan–Bengal fan denudation-accumulation system during the past 20Ma. *Journal of Geology*, **104**, 163–184.

ELDERFIELD, H., HAWKESWORTH, C. J., GREAVES, M. J. & CALVERT, S. E. 1981. Rare earth element geochemistry of oceanic ferromanganese nodules and associated sediments. *Geochimica et Cosmochimica Acta*, **45**, 513–528.

EMMEL, F. J. & CURRAY, J. R. 1984. The Bengal submarine fan, northeastern Indian Ocean. *Geo-marine Letters*, **3**, 119–124.

FRANCE-LANORD, C., DERRY, L. & MICHARD, A. 1993. Evolution of the Himalaya since Miocene time: isotopic and sedimentalogical evidence from the Bengal Fan. *In*: TRELOAR, P. J. & SEARLE, M. P. (eds) *Himalayan Tectonics*. Geological Society, London, Special Publications, **74**, 603–621.

GOLDBERG, E. D. & GRIFFIN, J. J. 1970. The sediments of

the northern Indian Ocean. *Deep Sea Research*, **17**, 513–537.

GOLDSTEIN, S. L. 1988. Decoupled evolution of Nd and Sr isotopes in the continental crust and the mantle *Nature*, **336**, 733–738.

—— & JACOBSEN, S. B. 1988. Nd and Sr isotopic systematics of river water suspended material: implications for crustal evolution. *Earth and Planetary Science Letters*, **87**, 249–265.

——, O'NIONS, R. K. & HAMILTON, P. J. 1984. A Sm-Nd isotopic study of atmospheric dusts and particulates from major river systems. *Earth and Planetary Science Letters*, **70**, 221–236.

GOVINDARAJU K. 1989. Compilation of working values and sample descriptions for 272 geostandards. *Geostandards Newsletter*, **XIII** (special issue), 1–113.

HANSEN, E. C., NEWTON, R. C., JANARDHAR, A. S. & LINDENBERG, S. 1995. Differentiation of late Archean crust in the Eastern Dharwar Craton, Krishnagiri-Salem area, south India. *Journal of Geology*, **103**, 629–651.

HARRIS, N. B. W., SANTOSH, M. & TAYLOR, P. N. 1994. Crustal evolution in south India: constraints from Nd isotopes. *Journal of Geology*, **102**, 139–150.

HARVEY, P. K., TAYLOR, D. M., HENDRY, R. D. & BANCROFT, F. 1973. An accurate fusion method for analysis of rocks and chemically related materials by X-ray fluorescence spectrometry. *X-ray Spectrometry*, **2**, 33–44.

HERRON, M. M. 1988. Geochemical classification of terrigenous sands and shales from core or log data. *Journal of Sedimentary Petrology*, **58**, 820–829.

INGERSOLL, R. V. & SUCZEK, C. A. 1979. Petrology and provenance of Neogene sands from Nicobar and Bengal fans, DSDP Sites 211 and 218. *Journal of Sedimentary Petrology*, **49**, 1217–1228.

JOHNSON, M. R. W. 1994. Volume balance of erosional loss and sediment deposition related to Himalayan uplifts. *Journal of the Geological Society, London*, **151**, 217–220.

JONES, B. & MANNING, D. A. C. 1994. Comparison of geochemical indices used for the interpretation of palaeoredox conditions in ancient mudstones. *Chemical Geology*, **111**, 111–129.

KOLLA, V. & BISCAYE, P. 1973. Clay mineralogy and sedimentation in the eastern Indian Ocean. *Deep Sea Research*, **20**, 727–738.

KUEHL, S. A., HARIU, T. M. & MOORE, W. S. 1989. Shelf sedimentaion off the Ganges–Brahmaputra river systems: evidence for sediment bypassing to the Bengal fan. *Geology*, **17**, 1132–1135.

LIGHTFOOT, P. C. 1985. *Isotope and Trace Element Geochemistry of the South Deccan Lavas, India.* PhD Thesis, The Open University, UK.

MAHONEY, J. J. 1988. Deccan traps. *In*: MACDOUGALL, J. D. (ed.) *Continental Flood Basalts*. Kluwer, Dordrecht, 151–194.

MARSH, J. S. 1991. REE fractionation and Ce anomalies in weathered Karoo dolerite. *Chemical Geology*, **90**, 189–194.

MARTIN, J. M. & MEYBECK, M. 1979. Chemical composition of river-bourne particulates. *Marine Chemistry*, **7**, 193–206.

MCLENNAN, S. M. 1989. Rare earth elements in sedimentary rocks: influence of provenance and sedimentary process. *Reviews in Mineralogy*, **21**, 169–200.

—— & HEMMING, S. 1992. Samarium/neodymium elemental and isotopic systematics in sedimentary rocks. *Geochimica et Comochimica Acta*, **56**, 887–898.

——, TAYLOR, S. R., MCCULLOCH, M. T. & MAYNARD, J. B. 1990. Geochemical and Nd-Sr isotopic composition of deep-sea turbidites: crustal evolution and plate tectonic associations. *Geochimica et Cosmochimica Acta*, **54**, 2015–2050.

——, HEMMING, S., MCDANIEL, D. K. & HANSON, G. N. 1993. Geochemical approaches to sedimentation, provenance, and tectonics. *In*: JOHNSON, M. J. & BASU, A. (eds) *Processes Controlling the Composition of Clastic Sediments*. Geological Society of America, Special Paper, **284**, 21–40.

MYERS, K. J. & WIGNALL, P. B. 1987. Understanding Jurassic organic-rich mudrocks- new concepts using gamma-ray spectrometry and palaeoecology: examples from the Kimmeridge Clay of Dorset and the Jet Rock of Yorkshire. *In*: LEGGETT, J. K. & ZUFFA, G. G. (eds) *Marine Clastic Sedimentology*. Graham & Trotman, London, 172–189.

NELSON, B. K. & DEPAOLO, D. J. 1988. Comparison of isotopic and petrographic provenance indicators in sediments from Tertiary continental basins of New Mexico. *Journal of Sedimentary Petrology*, **58**, 348–357.

NESBITT, H. W. 1979. Mobility and fractionation of rare earth elements during weathering of a granodiorite. *Nature*, **279**, 206–210.

—— & YOUNG, G. M. 1982. Early Proterozoic climates and plate motions inferred from major element chemistry of lutites. *Nature*, **299**, 715–717.

—— & —— 1984. Prediction of some weathering trends of plutonic and volcanic rocks based on thermodynamic and kinetic considerations. *Geochimica et Cosmochimica Acta*, **48**, 1523–1534

—— & —— 1989. Formation and diagenesis of weathering profiles. *Journal of Geology*, **97**, 129–148.

——, MAKOVICS, G. & PRICE, R. C. 1980. Chemical processes affecting alkalis and alkaline earths during continental weathering. *Geochimica et Cosmochimica Acta*, **44**, 1659–1666.

NEWTON, R. C. & HANSEN, E. C. 1986. The South India-Sri Lanka high-grade terrain as a possible deep-crust section. *In*: DAWSON, J. B., CARSWELL, D. A., HALL, J. & WEDEPOHL, K. H. (eds) *The Nature of the Lower Continental Crust*. Geological Society, London, Special Publications, **24**, 297–307.

PAUL, D. K., RAY BARMAN, T., MCHAUGHTON, N. J., FLETCHER, R., POTTS, P. J., RAMAKRISHNAN, M. & AUGUSTINE, P. F. 1990. Archean–Proterozoic evolution of Indian charnockites: isotopic and geochemical evidence from granulites of the Eastern Ghats belt. *Journal of Geology*, **98**, 253–263.

PEUCAT, J. J., VIDAL, P., BERNARD-GRIFFITHS, J. & CONDIE, K. C. 1989. Sr, Nd, and Pb isotopic systematics in the Archean low- to high-grade transition zone of southern India: syn-accretion vs post-accretion granulites. *Journal of Geology*, **97**, 537–549.

POTTS, P. J., TINDLE, A. G. & WEBB, P. C. 1992. *Geochemical Reference Material Compositions*. Whittles Publishing, Caithness.

RADHAKRISHNA, B. P. 1993. Neogene uplift and geomorphic rejuvenation of the Indian peninsula. *Current Science*, **64**, 787–793.

—— & NAQVI, S. M. 1986. Precambrian continental crust of India and its evolution. *Journal of Geology*, **94**, 145–167.

REA, D. K. 1992. Delivery of Himalayan sediment to the northern Indian Ocean and its relation to global climate, sea level, uplift and seawater strontium. *In*: DUNCAN, R. A., REA, D. K., KIDD, R. B., VON RAD, U. & WEISSEL, J. K. (eds) *Synthesis of Results from Scientific Drilling in the Indian Ocean*. American Geophysical Union, Geophysics Monograph **70**, 387–402.

SAGAR, W. W. & HALL, S. A. 1990. Magnetic properties of black mud turbidites from ODP Leg 116, distal Bengal fan, Indian Ocean. *In*: COCHRAN, J. R. & STOW, D. A. V. (eds) *Proceedings of the Ocean Drilling Program Leg 116, Scientific Results*. College Station, Texas, Ocean Drilling Program, 317–336.

SARKAR, G., CORFU, F., PAUL, D. K., MCNAUGHTON, N. J., GUPTA, S. N. & BISHUI, P. K. 1993. Early Archaean crust in Bastar Craton, central India – a geochemical and isotopic study. *Precambrian Research*, **62**, 127–137.

SHAW, D. M., CRAMER, J. J., HIGGINS, M. D. & TRUSCOTT, M. G. 1986. Composition of the Canadian Precambrian shield and the continental crust of the earth. *In*: DAWSON, J. B., CARSWELL, D. A., HALL, J. & WEDEPOHL, K. H. (eds) *The Nature of the Lower Continental Crust*. Geological Society, London, Special Publications, **24**, 275–282.

STOW, D. A. V., HOWELL, D. G. & NELSON, C. H. 1983. Sediment, tectonic and sea level controls on submarine fan and slope-apron turbidite systems. *Geo-Marine Letters*, **3**, 57–64.

——, AMANO, K., BALSON, P. S. *ET AL.* 1990. Sediment facies and processes on the distal Bengal fan. *In*: COCHRAN, J. R. & STOW, D. A. V. (eds) *Proceedings of the Ocean Drilling Program Leg 116, Scientific Results*. College Station, Texas, Ocean Drilling Program, 377-396.

TAYLOR, P. N., CHADWICK, B., MOORBATH, S., RAMAKRISHNAN, M. & VISWANATHA, M. N. 1984. Petrography, chemistry and isotopic age of Peninsular Gneiss, Dharwar acid volcanic rocks and the Chitradurga granite with special reference to the late Archaean evolution of the Karnataka Craton, southern India. *Precambrian Research*, **23**, 349–375.

TAYLOR, S. R. & MCLENNAN, S. M. 1985. *The Continental Crust: its composition and evolution*. Blackwell Scientific Publications, Oxford.

YOKOYAMA, K., AMANO, K., TAIRA, A. & SAITO, Y. 1990. Mineralogy of silts from the Bengal fan. *In*: COCHRAN, J. R. & STOW, D. A. V. (eds) *Proceedings of the Ocean Drilling Program Leg 116, Scientific Results*. College Station, Texas, Ocean Drilling Program, 59–73.